Chemical interactions between a sedimentary diapir and surrounding magma: evidence from the Phepane Dome and Bushveld Complex, South Africa

Revision 1

Rachel H. P. Ireland[1] and Sarah C. Penniston-Dorland[1,*]

[1]*Department of Geology, University of Maryland, College Park, MD 20742, USA*

**To whom correspondence should be directed: sarahpd@umd.edu*

Keywords: STABLE ISOTOPES: lithium isotopes, oxygen isotopes, FLUID PHASE: intergranular partial melt, aqueous fluid, DIFFUSION: lithium and oxygen, METAMORPHIC PETROLOGY, IGNEOUS PETROLOGY

Abstract

The Phepane Dome is a circular outcrop of metasedimentary rock within the Eastern Lobe of the Bushveld Complex hypothesized to have formed as a diapir, when underlying wallrock rose into the overlying magma body. Interactions between the metasedimentary rock of the Phepane Dome and the magma of the Bushveld Complex were investigated through measurements of oxygen and lithium isotopic compositions, determination of mineral modes and major-element mineral compositions, cathodoluminescence imaging, and dihedral angle analysis. Evidence from cathodoluminescence imaging and dihedral angle analysis suggest that heat transfer during diapirism caused partial melting and complete recrystallization of the Phepane Dome metasedimentary rock. Oxygen isotope analysis of samples from traverses spanning the contact between metasedimentary and igneous rocks demonstrates that relatively minimal exchange of oxygen (over distance ~4 m) occurred across the contact between the Phepane Dome and the surrounding Bushveld magma. The lithium concentrations and isotopic compositions of metasedimentary rock are significantly different from the associated igneous rocks. Lithium isotope analysis of samples from traverses across the contact demonstrates exchange of Li over somewhat greater distances (~60 m) than oxygen, consistent with evidence that suggests a higher diffusivity of Li than most major elements. Models of oxygen diffusion through intergranular melt and aqueous fluid are used to place maximum constraints on the duration of diffusive exchange across the contact, resulting in estimates ranging from 5 kyrs to 5 Myrs. These values are consistent with previous estimates of the duration of crystallization of the Bushveld Complex and Phepane diapir development.

Introduction

The largest layered mafic intrusion in the world, the Bushveld Complex of South Africa, formed as mafic to ultramafic magma intruded sedimentary rocks of the Transvaal Supergroup ~2054 Ma (Walraven et al., 1990; Buick et al., 2001) (Figure 1a). Metasedimentary domes found within the mafic rock of the Eastern Lobe of the Bushveld Complex are interpreted to have formed as diapirs of partially melted, sedimentary footwall rock that rose through the denser mafic magma (Uken and Watkeys, 1997) (Figure 1b). Evidence for this sedimentary diapirism comes from gravity and structural data (Molyneux and Klinkert, 1978). The Phepane Dome crops out as one of these domal structures of metasedimentary rock surrounded by Bushveld Complex rock in the northern Eastern Lobe and shows both structural and mineralogic evidence for a diapiric origin (Johnson et al., 2004).

Gerya et al. (2003, 2004) described the formation of the Phepane Dome as "cold diapirism," since cooler, less dense sedimentary rock rose into the hotter, denser Bushveld Complex crystallizing magma. Similar "cold diapirism" is hypothesized to occur in subduction zones (Hall and Kincaid, 2001; Gerya and Yuen, 2003). To better understand this cold diapirism within the Bushveld Complex magma, studies have modeled the growth of the Phepane diapir (Gerya et al., 2004) and documented the metamorphic reactions that occurred in the sedimentary rock at the center of the Phepane Dome (Johnson et al., 2004). However, there is limited study of these thermally dynamic settings where chemical buoyancy plays such an important role. This study investigates chemical interaction between the Bushveld Complex magma and the sedimentary rock that rose as the Phepane diapir using Li and O isotopes as chemical tracers.

The properties of Li, a fluid-mobile element with a ~17% mass difference between the two stable isotopes (^{6}Li and ^{7}Li), make it a useful tracer for settings where fluids and rock interact. Recent studies have reported Li isotopic compositions and concentrations in contact metamorphic settings (e.g., Teng et al. 2006a; Marks et al., 2007), and O isotope data has been used in previous studies of intrusion-wallrock contacts (e.g., Shieh and Taylor, 1969; Cartwright and Valley, 1991; Park et al., 1999; Baumgartner and Valley, 2001). During contact metamorphism, the juxtaposition of two chemically disparate rock types at relatively high temperatures can lead to chemical or isotopic exchange across the contact. Such mass transfer between the two reservoirs is facilitated by diffusion due to gradients in chemical potential. The extent of the transfer relies on a number of physical properties of the exchange media as well as on the length of time the two reservoirs are in contact at high temperatures. Therefore, analysis of the diffusive distance across the contact can elucidate information about the time the two reservoirs were able to exchange. This study measures Li compositions and O isotopic compositions across the Phepane Dome-Bushveld Complex contact in order to determine the extent of diffusive exchange and constrain the timescale of diffusion and diapiric formation. It is the first to use both Li and O as chemical tracers of diffusion, directly comparing the two systems and providing an important assessment of each system at the same contact metamorphic setting. It is also an important corollary to the experimental studies that show that Li will diffuse orders of magnitude faster than other components in basaltic and rhyolitic melts (Richter et al., 2003).

Geologic Background

Bushveld Complex

The mafic-ultramafic Rustenburg Layered Suite of the Bushveld Complex intruded into the Transvaal Basin of South Africa (Figure 1a) at ~2054 Ma in stages of multiple magma injections into the clastic and chemical sedimentary rocks of the Transvaal Supergroup (Cawthorn and Walraven, 1998; Walraven et al., 1990; Buick et al., 2001; Scoates and Friedman, 2008). The stages resulted in five compositional zones: the Marginal, Lower, Critical, Main, and Upper Zones. During crystallization of each stage, the magma fractionated to form layers of variable mafic compositions (Cawthorn and Walraven, 1998). The Lebowa Granite Suite and Rashoop Granophyre are adjacent to the Rustenburg Layered Suite and comprise the more felsic intrusive portion of the Bushveld Complex (Hill et al., 1996; Schweitzer et al., 1997; Fourie and Harris, 2011). A minimum preferred age of 2049 +69/-75 Ma for the Lebowa Granite Suite is resolved from separate intrusions with similar Pb-Pb isochron ages (Walraven et al., 1990). Important ore concentrations are found throughout the Bushveld Complex, including 75% of the world's Pt reserves and 50% of the world's Pd reserves (Cawthorn, 1999).

The Transvaal Supergroup sediments were deposited onto the Kaapvaal Craton, and consist of Archean protobasinal rocks overlain by the Black Reef Formation, the Chuniespoort Group carbonates and banded iron formation, and the Proterozoic age Pretoria Group (Eriksson et al., 2001). The depositional age of Pretoria Group sedimentary rocks is constrained by a Re-Os age of pyrite from carbonaceous shale of the Timeball Hill Formation of 2316 ± 17 Ma (Hannah et al., 2004).

Phepane Dome

Within the Eastern Lobe of the Bushveld Complex, the eroded Phepane Dome forms a topographic bowl-like structure of meta-sedimentary rocks (Figure 2). These rocks have been correlated to the Pretoria Group formations of the Transvaal Supergroup (Johnson et al., 2004). The outer quartzite directly in contact with the Bushveld Complex igneous rocks has been correlated to the Lakenvalei Formation. The Lakenvalei is in contact with Upper Zone mafic rocks on the western side of the Phepane Dome, while the Lakenvalei on the eastern and southern sides is in contact with felsic rocks, likely of the Lebowa Granite Suite. The timing of the felsic magmatism compared to the mafic magmatism at the Phepane Dome is uncertain. Continuing towards the center of the Phepane Dome, the Vermont, Magaliesburg, and Silverton Formations are observed (Johnson et al., 2004). The Vermont Formation consists of metapelitic rock with calc-silicate layers. The top of the Phepane Dome bowl-like ridge is the resistant Magaliesburg quartzite, with the less resistant Silverton pelitic hornfels in the middle of the bowl.

Diapirism in the Eastern Lobe

The contact aureole of the Bushveld Complex is thickest in the northern part of the Eastern Lobe, extending 5 km down into the underlying sedimentary rock (Uken and Watkeys, 1997; Clarke et al., 2005). It is thought that the thickness of the contact aureole directly relates to the occurrence of pericline folding and meta-sedimentary domes (Clarke et al., 2005). Water released from the sedimentary rocks farthest away in the aureole caused anatexis in the overlying suprasolidus rock closest to the contact (Harris et al., 2003; Johnson et al., 2003). Partial melting of the sedimentary rock combined with the finger-like intrusion style of the Lower Zone created nucleation points for diapirism, e.g. the Phepane Dome, and caused folding of the partially melted sedimentary rocks, e.g. the Steelpoort and Derde Gelid periclines at the Burgersfort Bulge (Clarke et al., 2005) (See Figure 1b). Diapirism is believed to be triggered by crustal loading under the long finger-shaped injections of denser mafic magma, with diapirs initiating in the sedimentary rock inter-finger areas (Uken and Watkeys, 1997).

Evidence for diapirism comes from the combination of structural, gravity, and mineralogic data. Molyneux and Klinkert (1978) concluded that mafic rock exists beneath the sedimentary rocks of the Malope Dome and the Marble Hall structure in the southern region of the Eastern Lobe based on gravity data. Combining this gravity data with structural data at the Malope Dome, Molyneux and Klinkert (1978) concluded that the 30° outward dip was too shallow to explain the underlying mafic rock if Malope formed as a simple dome and inferred a diapiric origin of the structure. At the Phepane Dome, the almost vertical alignment of curtain folds and lineations in the core compared to shallow alignments in the outer layers indicates bulbous formation as a diapir (Uken and Watkeys, 1997; Johnson et al., 2004). Additionally, the mineral assemblage of the meta-sedimentary rocks in the core of the Phepane Dome is consistent with the occurrence of partial melting within the dome at temperatures greater than 720°C (Johnson et al., 2004). The preserved spinel and cordierite symplectites replacing andalusite in the core of the Phepane Dome suggests that decompression occurred during the thermal peak as the diapir rose into the Bushveld Complex magma (Johnson et al., 2004).

Timescale of diapirism

Previous studies have estimated the timescales of Bushveld Complex formation and cooling (Cawthorn and Walraven, 1998; Nomade et al., 2004; Scoates and Friedman, 2008) and Phepane diapirism (Gerya et al., 2004). Cawthorn and Walraven (1998) use a thermal model to determine the amount of time a 7.5 km thick intrusion the size of the Bushveld Complex would require to cool and crystallize. In their model, they simulated a series of intrusions by adding layers of magma into wallrock and used equations of conductive heat flow to determine the vertical changes in heat content across these layers for small increments of time. After 180 kyrs, the entire intrusion cooled to less than the assumed solidus temperature of 900°C, rendering the intrusion completely crystallized by 200 kyrs. This would prohibit further diapiric rise, indicating that the Phepane Dome diapir would have formed within the 200 kyr time period. Gerya et al. (2004) use inferred viscosity and thermal properties of the sedimentary rock and heat flow associated with the Bushveld Complex magma to predict the development of the Phepane diapir. Their preferred model results in a 200-300°C gradient from the cooler core to hotter rim of the diapir. The termination of diapir growth occurs when the viscosity of the Bushveld magma becomes too great as solidification occurs at less than 900°C. Gerya et al. (2004) found the formation of the diapir within the hotter mafic rock to be plausible in one million years. Measurements of overlapping U-Pb crystallization ages of zircon (closure temperature > 950°C; Cherniak and Watson, 2000) and rutile (closure temperature ~720-800°C, using formulation of Dodson, 1973, and Pb diffusion data of Cherniak, 2000) are consistent with rapid cooling of 100ºC to 1000ºC/m.y. (Scoates and Friedman, 2008). Also, $^{40}Ar/^{39}Ar$ ages of biotite suggest that cooling from 700 to <500°C is also rapid (Nomade, et al., 2004).

The two models described above present time estimates for the Phepane Dome formation as a diapir (cooled to ~900°C) in 200 kyrs and 1 Myrs. This study evaluates the plausibility of the two given time estimates by measuring O and Li isotopic compositions across a contact between the Phepane Dome and the Bushveld Complex to determine the extent of diffusive exchange. If sufficient cross-contact exchange has occurred, the results can be fit with a numerical diffusion model. The best fit model to the data will constrain the amount of time that lithium and oxygen exchange occurred in this system, and therefore provide a maximum constraint to the duration of the Phepane diapir formation.

Analytical Methods

Samples were collected in four transects across the contact between the Phepane Dome and the Bushveld Complex; two each on the eastern and western sides (Figure 2). Samples were also collected from the Pretoria Group in the outer aureole of the Eastern Lobe (See Figure 1b). Four samples were collected from the Lakenvalei Formation, and one sample was taken from the Vermont Formation. The locations of samples were recorded as GPS coordinates at the time of sampling, with smaller-scale distances measured relative to the contact between igneous rock and metasedimentary rock using measuring tape oriented perpendicular to the quartzite-igneous rock contact (Table 1).

Modal abundances of minerals in representative samples were determined by point counting of thin sections from each rock type on the JXA-8900 Electron Probe Microanalyzer (EPMA) at the University of Maryland. Backscatter electron imaging was used with an energy dispersive X-ray spectrometer to identify each phase. For each sample, ~2000 points were counted in a grid of 0.5 mm spacing. Major element compositions of plagioclase were also obtained using the EPMA. Plagioclase was analyzed using a beam current of ~20 nA with an accelerating voltage of 15 keV and a 10μm spot size. The weight percent of each element was calculated from raw intensities using a ZAF correction. Natural silicate mineral standards were analyzed at the beginning and end of an analytical day for standardization.

Samples of Lakenvalei Quartzite and Sandstone were analyzed by Cathodoluminescence (CL) imaging at the Smithsonian Institute Department of Mineral Sciences. The CL system utilizes an ELM 3R Luminoscope with a 17 kV electron beam and 500 μA current, connected to an optical microscope. Pictures were taken using the program MagnaFIRE with an Olympus camera that allows for an extended exposure time to acquire the low luminescence of quartz.

The oxygen isotopic compositions of quartz and feldspar mineral separates and whole rock powders were measured for samples from the East Phepane 06 and the West Phepane Small Scale Transects. Quartz separates were rinsed in concentrated HF for 30 seconds and dried to check for feldspar contamination. The feldspar separates were crushed to powder and analyzed using X-ray diffraction at the University of Maryland X-ray Crystallographic Center to ensure purity. Samples were then measured for oxygen isotopic composition at the University of Wisconsin-Madison Stable Isotope Laboratory. Between 1 and 2 mg of material for each sample was treated overnight at room temperature in the sample chamber with BrF5, then individually heated with a CO_2 laser in the presence of BrF_5 to release O_2, which was cryogenically purified, converted into CO_2 and analyzed on a dual inlet five collector Finnigan MAT 251 mass spectrometer. Results are reported as $\delta^{18}O$ relative to standard mean ocean water (VSMOW). Accuracy and analytical precision were verified during each set of analyses by multiple analyses of the Gore Mountain garnet standard (UWG-2). Raw standard $\delta^{18}O$ values for each session were corrected to the accepted value for UWG-2 ($\delta^{18}O$= 5.8‰, Valley et al., 1995). The average uncorrected $\delta^{18}O$ value (± 2 S.D.) of UWG-2 for the two run sessions were 5.63±0.08‰ and 5.81±0.05‰.

The lithium concentrations and isotopic compositions of each sample were determined by measuring whole rock powders. Each sample was cut to find the freshest piece and powdered in the Mixer Mill 8000 using a tungsten carbide container in the Geochemistry Labs at the University of Maryland. Dissolution of the powders was conducted using the method of Rudnick et al. (2004), with an additional concentrated hydrochloric and nitric acid aqua-regia step. Using a method similar to Moriguti and Nakamura (1998), the resultant solution is passed through three cation exchange columns in order to separate Li for analysis. Finally, the samples were analyzed using the Nu Plasma Multi Collector-Inductively Coupled Plasma-Mass Spectrometers (MC-ICP-MS) at the University of Maryland and the Carnegie Institution of Washington according to the method described in Teng et al. (2004). Results are reported as δ^7Li relative to the standard L-SVEC. Long-term reproducibility of Li isotopic measurements is within ±1‰ (2σ) as determined by Teng et al. (2004), and verified through analysis of Li solution standards UMD-1 (+54.7‰) and IRMM-016 (-0.1‰) during each analytical run. The average δ^7Li value for all measurements at the University of Maryland of UMD-1 is 54.7±0.9‰ (2σ, n=26) and for IRMM-016 it is 0.5±1.0‰ (n=21). The average δ^7Li value for all measurements at the Carnegie Institution of Washington of UMD-1 is 55.0±0.4‰ (2σ, n=2) and for IRMM-016 it is -0.1±0.3‰ (n=5). Measured ^{7}Li voltages for samples are compared to the ^{7}Li voltage measured for the 50 ppb L-SVEC standard to determine the concentration of Li in solution and then adjusted for the mass of each sample powder dissolved to determine the rock Li concentration. This results in values for Li concentration with 2σ uncertainties of <±10% (Teng et al., 2006b) for standard materials. Variations in concentration above that uncertainty were measured in replicate analyses of samples for this study. This variation is most likely due to heterogeneity of the rock samples and could result from incorporation of different amounts of relatively Li-rich low-abundance phases, such as chlorite or even fluid inclusions. Isotopic compositions were more homogeneous than Li concentrations with all measurements falling within 1‰ uncertainty (2σ) of the average.

Two basalt standards (BHVO-1 and BHVO-2) were dissolved and processed through the cation exchange columns. Two measurements of BHVO-1 at the University of Maryland resulted in an average δ^7Li of 4.1‰ and Li concentration of 5.2 ppm. Three BHVO-2 analyses at the University of Maryland resulted in an average δ^7Li of 3.6‰ and Li concentration of 4.9 ppm. One BHVO-2 analysis at the Carnegie Institution of Washington resulted in a δ^7Li of 4.4‰ and

Li concentration of 4.4 ppm. These results fall within uncertainty of previous measurements of the Li concentration and δ^7Li of these standards. Previously reported measurements of δ^7Li for BHVO-1 range from +4.0 to +6.1‰ and from 4.0 to 5.4 ppm and for BHVO-2 from +4.0 to +5.5‰ with reported concentrations ranging from 4.1 to 4.8 ppm in the literature (see GeoReM database, http://georem.mpch-mainz.gwdg.de/).

Results

Petrology

Quartzite samples from the East and West side of the Phepane Dome consist predominantly of quartz with <15% alkali feldspar and plagioclase feldspar, minor (<3%) amounts of muscovite and chlorite and trace calcite, zircon, apatite, rutile and monazite (Table 2). The Bushveld Complex felsic igneous rock is hornblende-bearing granite with a small amount of biotite and trace amounts of zircon, Fe-Ti oxides and phosphates. The mafic rock is amphibolitized gabbro or quartz gabbro comprised mostly of labradorite (average plagioclase composition of An_{68}, see Table 3) and hornblende ± pyroxene.

Quartz Cathodoluminescence

Cathodoluminescence (CL) exposes growth zoning and annealed micro-cracks and fractures in quartz that are not optically visible, revealing evidence for the history of mineral growth and/or late stage fluid infiltration events (Valley and Graham, 1996; Penniston-Dorland, 2001; Harris et al., 2003). Recrystallization events can change the trace element abundance and defects in the crystal lattice of the quartz, two properties thought to be activators of luminescence (Götze et al., 2001). Examination under CL can show if the quartz from the Lakenvalei quartzite in the Phepane Dome has retained its original sedimentary CL response, has been partially or completely recrystallized due to the contact metamorphism, and whether there was later recrystallization due to a late stage fluid infiltration.

To identify the characteristic CL response of Lakevalei sedimentary protoliths, sample LV4 from the Lakenvalei Sandstone was imaged (Figure 3a,b). This sample has mostly non-luminescing detrital quartz grains, with occasional heterogeneous blue luminescing detrital grains. Bright red-luminescing authigenic quartz is seen between detrital grains and along some grain boundaries, and a non-luminescent cement is visible. The mixture of detrital grains and low- or red-luminescent cement is common for sedimentary rocks (Götze et al., 2001).

In contrast, quartz grains from the Lakenvalei Quartzite generally luminesce bright blue (Figure 3c: regions labeled B), showing no evidence of the sedimentary signature. There is also a darker blue luminescence that usually occurs in within grains, separating multiple regions of smaller bright blue luminescence within individual quartz grains (Figure 3c, regions labeled L). Non-luminescent quartz is also recognized both in association with abundant fluid inclusions and along fractures with few or no fluid inclusions (Figure 3c-h). The non-luminescent quartz associated with fluid inclusions appears in samples from both sides of the Phepane Dome, occurring within grains, at grain boundaries and following fractures. Most non-luminescent zones are relatively narrow compared to the size of the grains. The non-luminescent quartz not associated with fluid inclusion trails in some cases cuts both feldspars and quartz and is only found in samples from the East side (Figure 3g-h). These fractures must have occurred late, because they are associated with visible fracturing and have relatively few or no fluid inclusions. There are few appearances of this texture.

Dihedral angle analysis

To confirm that these Phepane Dome samples could indeed have been partially melted, the measurement of quartz-quartz-feldspar dihedral angles in thin sections from all transects was used. This method was used by Harris et al. (2003) to recognize the former presence of melt in the outer aureole of the Bushveld Complex Eastern Lobe. Harris et al. (2003) measured more than 25 dihedral angles at quartz-quartz-feldspar grain junctions in thin sections of the Lakenvalei and Magaliesburg Quartzites, observing a two peaked distribution: one peak of angles in the ~90° range, and one peak of angles in the 105-110° range. Feldspar angles of 105-110° are representative of solid state equilibrium between phases (Vernon, 1968), while angles less than this are associated with partial melt and subsequent crystallization (Holness, 2006). Harris et al. (2003) concluded that the distribution of angles they observed corresponds to a solid-state equilibrium dihedral angle and a lower, melted feldspar dihedral angle. This represents heterogeneous melting of feldspars at the grain scale in their rocks.

Thin section analysis of six Lakenvalei quartzites shows both populations of dihedral angles with a similar two peaked distribution, indicating that melt was present during the formation of the Phepane diapir (Figures 4, 5). Two thin sections (P06-18 and P07-26) show two obvious peaks in the angle measurements, with a peak in the lower range at ~50° indicative of partial melting and a peak at ~105° indicative of solid state equilibrium. The dihedral angles measured in thin sections from samples closest to the contact (P06-15 and P07-30) are more scattered. This could be due to the optical measurement of thin sections that only records 2-D angles and not the true 3-D dihedral angle. Harris et al. (2003) reported that the median of >25 measured 2-D angles in one thin section is within 1° of the 3-D angle. The 3-D dihedral angles of two samples were measured using a universal stage and compared to the results from the 2-D measurements to verify this accuracy. The results of measurements with the universal stage revealed an abundance of low angles with a peak at ~40°, indicating that the 2-D measurement method has spread these angles over 20-90°. In addition, measurements of angles in P06-18 using both the 2-D method and the universal stage show the same two-peaked distribution (Figure 5). Thus, the dihedral quartz-quartz-feldspar angles in metasedimentary rocks of the Phepane diapir record partial melting during formation.

Oxygen isotopic compositions

The oxygen isotopic compositions of samples from each rock type are shown in Table 4 and Figure 6. The average $\delta^{18}O$ of the Lakenvalei quartz is 11.2 ± 0.4‰ on the East side and 10.9 ± 0.6‰ on the West side (all ranges are 2 standard deviations). These values fall within the range determined by Harris et al. (2003) for quartz from the Lakenvalei and Magaliesburg Quartzites in the outer aureole of the Eastern Lobe (11.8±0.5‰) and the one Lakenvalei Quartzite sample (11.06 ± 0.2‰) measured by Schiffries and Rye (1989). Quartz from the felsic Bushveld Complex igneous rock adjacent to the Phepane Dome has $\delta^{18}O$ values of 7.3 ± 0.8‰. This value is consistent with $\delta^{18}O$ values of quartz in Bushveld granites and granophyres (7.95 ± 1.03 ‰) reported by Fourie and Harris (2011). On the West side, the feldspar and whole rock powders of the mafic Bushveld Complex igneous rock yielded similar $\delta^{18}O$ of 8.1 ± 0.6‰ and 7.6 ± 1.2‰ respectively. The $\delta^{18}O$ range of plagioclase separates from this study (8.1 ± 0.6‰) is within the range of Bushveld plagioclase (7.5 ± 1.2‰) measured by Harris et al. (2005) and the range (7.6 ± 0.3‰) measured by Schiffries and Rye (1989). These studies interpreted the oxygen isotope compositions as unaltered by a secondary fluid, since the fractionation between pyroxene and plagioclase $\delta^{18}O$ values resulted in the calculation of magmatic temperatures (~1000°C).

The oxygen isotopic compositions of the minerals in each rock type appear to be mostly homogeneous, with constant $\delta^{18}O$ far from the contact (see Figure 6). Samples closest to the contact on either side of the contact exhibit variations consistent with isotopic exchange across the contact (i.e. elevated $\delta^{18}O$ in igneous rock and lowered $\delta^{18}O$ in the metasedimentary rock adjacent to the contact). To compare the $\delta^{18}O$ of quartz from the Lakenvalei Quartzite with the $\delta^{18}O$ values of plagioclase in the mafic rock, the oxygen isotope composition of fictive quartz in equilibrium with the mafic Bushveld Complex rock can be calculated from the measured plagioclase values in the West Small Scale Transect using the fractionation factors for quartz-anorthite and quartz-albite from Clayton and Kiefer (1991) and using mass balance to calculate the fractionation for quartz-labradorite. For likely temperatures in the Phepane Dome (>720°C; Johnson et al., 2004), the fictive quartz would be ~9.5‰. At 900°C, just under magmatic temperatures, the fictive quartz in the mafic rock is ~9‰.

This temperature of 900°C is used as the solidus temperature at which the Bushveld Complex magma would be completely crystallized in the model of Bushveld Complex cooling and crystallization (Cawthorn and Walraven, 1998). It also represents the temperature of "freezing in" of the diapir, as determined by the model of the formation of the Phepane diapir (Gerya et al., 2004). Assuming that there was no hydrothermal alteration, and that the addition of the cooler Phepane diapir rock would aid in a locally rapid cooling of the Bushveld magma, the preferred $\delta^{18}O$ values for quartz are the calculated values at 900°C. Subsolidus exchange between minerals is possible, but exchange is likely halted as the system cooled quickly due to the influence of the cooler Phepane diapir. Thus, the minerals would record a higher temperature fractionation compared to slowly cooled systems (e.g., Giletti, 1986). Schiffries and Rye (1989) found two Upper Zone samples with differences in plagioclase and orthopyroxene $\delta^{18}O$ values that suggest temperatures of 960°C and 1040°C. Samples measured by Harris et al. (2005) for Upper Zone rocks show a similar range in inferred temperatures. Therefore, using a temperature of 900°C is supported by these studies.

Lithium compositions

Results of the Li whole rock concentrations and isotopic compositions are reported in Table 5 and illustrated in Figures 7 and 8. The felsic Bushveld Complex has the lowest concentration of Li, with a relatively constrained range of 5.0 ± 4.0 ppm (all ranges are 2 standard deviations). This differs from the mafic Bushveld Complex rock, which is more varied in concentration (30 ± 36 ppm). The Lakenvalei Quartzite has a range of Li concentrations of 15 ± 7 ppm (see Figure 7 for plots of the East and West sides). The Vermont Metapelite is the most heterogeneous with Li concentrations ranging from 14 to 105 ppm, with an average Li concentration of 67 ppm. This variation is likely due to preservation of the initial heterogeneity in the protolith Vermont Shale, which is known to have sandstone- and calc-silicate-rich layers. Lastly, two analyses of the Magaliesburg Quartzite resulted in Li concentrations of 13 and 8.8 ppm.

The δ^7Li values in each rock type are variable, resulting in large ranges (see Table 5 for compositions and Figure 8 for plots of δ^7Li with distance in each transect). The felsic rock has an average δ^7Li value of 5.9 ± 5.8‰ (all ranges are 2 standard deviations), the Vermont Metapelite has an average of 3.5 ± 8.2‰, and the mafic rock has a similar average value of 3.7 ± 3.6‰. The Lakenvalei Quartzite is higher on the East side with an average δ^7Li of 19 ± 7‰ on the East side and 13 ± 8‰ on the West side.

Measurements of the sedimentary protolith concentrations (Table 5) correlate with their respective metasedimentary concentrations in the Phepane Dome. Four analyses of the Lakenvalei Sandstone gave δ^7Li values of 9.8‰, 12.4‰, 21.7‰ and 17.3‰ and concentrations of 2.3, 8.3, 9.1 and 13 ppm. The δ^7Li values are all within the range of Lakenvalei Quartzite δ^7Li compositions, but the Lakenvalei Sandstone Li concentrations are slightly lower overall compared to the Lakenvalei Quartzite concentrations. One analysis of the Vermont Shale resulted in a concentration of 142 ppm, consistent with the high concentrations found in the Vermont Metapelite. The δ^7Li of the Vermont Shale is 0.3‰, lower than most metapelite samples, but this is only one sample and cannot be extrapolated to the entire Vermont Shale δ^7Li composition.

Measurements of quartz mineral separates from the Lakenvalei Quartzite resulted in Li concentrations (20 ± 7 ppm) and δ^7Li values (19.4 ± 6.0‰). These values overlap with whole rock Li compositions (Table 5).

Discussion

Intergranular media and crystallization history: evidence from dihedral angles and cathodoluminescence

Diffusion that occurs due to a sharp compositional discontinuity across a contact requires chemical transport through the rock (Watson and Baxter, 2007). In the absence of advection, this is likely to be diffusive transport of the element or isotope of interest through an intergranular medium; volume diffusion through the solid would be too slow for a near surface contact metamorphic event (Cartwright and Valley, 1991). The type of intergranular medium (dry grain boundaries, fluid, or melt) will affect the diffusivity of the element or isotope, so the potential intergranular media at the Bushveld Complex-Phepane Dome contact are investigated.

The dihedral angle analysis of Lakenvalei quartzite samples from both sides of the Phepane Dome indicates that the Lakenvalei had partially melted at the grain-scale during formation. If partial melt was present and interconnected at the contact between the Phepane Dome and the Bushveld Complex, it would have facilitated diffusive exchange. Holness (1998) determined that dihedral angles must be lower than 60° for the intergranular melt to be connected. The low angle peak of dihedral angles measured by the 3-D method is ~40° (~50° by the 2-D method). This suggests that partial melt in the Lakenvalei would have been connected along grain boundaries, allowing for across-contact diffusive exchange.

The numerous fluid inclusions in quartz and feldspar from both the Phepane Dome and the Bushveld Complex rock indicate the presence of a fluid. Thin section analysis shows that fluid inclusions are commonly secondary, concentrating along fractures that cut across multiple quartz grains. In some cases these late, planar fluid inclusions are also associated with non-luminescing quartz, suggesting a later, low-temperature interaction of the rocks with fluids. However, these late non-luminescing bands are not abundant, suggesting that low-temperature recrystallization of quartz was not a significant event in the history of these rocks.

Cathodoluminescence imaging shows that some of the fluid inclusions can be related to a recrystallization event during contact metamorphism. As seen in Figures 3c-d fluid inclusions follow the curved region of darker luminescent blue that surrounds a region of bright blue. Since this assemblage of fluid inclusions is not linear, it is unlikely that the fluid inclusions formed in response to a fracture-healing event. Instead, the inclusions were likely a pore fluid that was trapped, indicating that the bright blue represents an earlier-formed quartz grain and the darker blue is an overgrowth during recrystallization in the presence of fluid. A similar darker blue luminescence occurs along grain boundaries of bright blue luminescent quartz in grains without fluid inclusions. Because the fluid inclusion density and the abundance of darker luminescence increase in samples closer to the contact (e.g. Figures 3g-h), it is likely that the darker luminescence is related to recrystallization at grain edges in the presence of fluid, with the samples near the contact experiencing more fluid and/or recrystallization during this stage than samples farther from the contact.

The colors and textures of CL are indicative of three different stages of metamorphism. The first is related to the bright blue luminescence and probably occurred as the Lakenvalei sandstone partially melted and metamorphosed during Bushveld Complex intrusion. Bright blue luminescence is thought to be related to crystallization or recrystallization at high temperature. Sprunt et al. (1978) found that quartz from contact metamorphic rocks in the Bergell Alps luminesced the most blue of metamorphic rocks, and Boggs et al. (2002) found that volcanic, plutonic, and contact metamorphic quartz all luminesced bright blue. More recent studies (e.g., Rusk et al., 2008) have hypothesized that Ti causes the bright blue luminescence because it preferentially substitutes for Si in quartz at higher temperatures and is abundant in magmatic settings. The bright blue luminescence and lack of a preserved sedimentary signature in the Lakenvalei quartzite suggests complete recrystallization of the quartz during contact metamorphism.

The second stage of quartz recrystallization formed the darker blue luminescence that is found within large grains separating regions of brighter luminescence. This recrystallization is likely related to contact metamorphism as well, and could have occurred as a fluid was released during crystallization of the magmas. This is supported by the greater abundance of fluid inclusions coinciding with darker blue luminescence in samples closer to the contact on the East side. In addition, quartz grains adjacent to aggregates of sheet silicates and feldspar usually only show the darker blue luminescence, suggesting that the fluid is also related to the formation of chlorite in the Lakenvalei Quartzite. The final recrystallization stage created the fracture-related non-luminescent quartz and is not as widespread as the other stages, suggesting minor late-stage fluid infiltration. The maximum abundance of this type of quartz CL is ~5% near the contact. The associated fracturing must have occurred after complete crystallization, since fractures cross cut both feldspars and quartz. This small amount of late stage fluid infiltration is negligible compared to the dominant recrystallization texture of blue luminescence. Thus, it is likely that both fluid and a partial melt were present as intergranular media during high-temperature contact metamorphism and diapirism of the Phepane Dome, and since late stage fluid infiltration appears to have been relatively minor, earlier across-contact diffusive exchange would not have been significantly affected by it.

Oxygen isotopic compositions

The $\delta^{18}O$ values of these Bushveld Complex mafic rocks (whole-rock average $\delta^{18}O$ = 7.6‰) are higher than typical mantle derived rocks (~5.7‰, Ito et al., 1987; Eiler, 2001) indicating interaction of the mafic rock with crustal rocks or fluids. However, these ^{18}O-enriched compositions are found in mafic rocks throughout the entire Bushveld Complex and have been interpreted to be a product of crustal contamination (Schiffries and Rye, 1989; Harris et al., 2005). Although the concurrent felsic magmatism could have been derived from the mafic Bushveld Complex or sedimentary rocks of the contact aureole, the oxygen isotopic compositions do not support either of these hypotheses (Fourie and Harris, 2011). The marked difference between the measured $\delta^{18}O$ of quartz in the metasedimentary rock (average 11.2‰) and that of the felsic rock (average 7.3‰) precludes the sedimentary aureole rocks as a source for this magma, consistent with the conclusions of Fourie and Harris (2011). Additionally, the oxygen isotope composition of quartz separates from the felsic rock (7.3‰) does not agree with the fictive quartz values in the mafic rock, which must be greater than the measured plagioclase values ($\delta^{18}O$= ~8.1‰) and are likely ~9.2‰. Thus, the oxygen isotopic composition of the metasedimentary rocks of the Phepane Dome do not suggest large-scale interaction of the dome with the Bushveld Complex, and the oxygen isotopic composition of the felsic rock suggests it is not genetically related to either the Phepane Dome metasedimentary rock or the mafic Bushveld rock.

The distinct oxygen isotopic compositions of the Lakenvalei Quartzite and the Bushveld Complex igneous rock show a relatively small-scale gradient in $\delta^{18}O$ that suggests diffusion of oxygen through an intergranular medium across the Bushveld Complex-Phepane Dome contact (Fig. 6). Evidence from quartz CL suggests that there was not significant late-stage fluid infiltration that might have overprinted $\delta^{18}O$ compositions of these rocks. The lack of significant secondary alteration implies that a high-temperature diffusive profile in $\delta^{18}O$ compositions across the contact of the Bushveld Complex and Phepane Dome would have been preserved.

The CL evidence also suggests that minerals were completely recrystallized by the high-temperature event and therefore the minerals would have recorded the isotopic composition present within an intergranular fluid (or fluids) due to across-contact exchange. While it is possible that there was isotopic exchange between quartz and other minerals during cooling, it is not a likely explanation for the observed isotopic gradient. Closure temperatures for quartz were calculated following Dodson (1973) with the following assumptions: a grain radius of 1 mm, a cooling rate of 100ºC/Myr, grains are spheres, values for D_0 and E taken from Giletti and Yund (1984) for α-quartz. The closure temperature using these values is ~515ºC which suggests that the oxygen isotopes in quartz could be open to post-crystallization exchange during cooling. However such post-crystallization exchange would affect mineral compositions but by itself would not affect whole-rock $\delta^{18}O$ values. The presence of a gradient in whole-rock $\delta^{18}O$ in mafic rocks along the West small-scale traverse argues against post-crystallization isotopic exchange as the cause for the observed isotopic gradients. Therefore this possibility is not considered in the following models.

The distinctly different oxygen isotopic compositions of the Lakenvalei Quartzite and the Bushveld Complex igneous rock and the similarity in isotopic composition of the igneous rocks to other unaltered rocks from the region preclude large-scale (> ~4 m) interaction between these rocks. These characteristics also suggest that significant fluid advection across the contact did not occur during or after the intrusive event. Other studies of oxygen isotopic compositions at wallrock-intrusion contacts measured diffusive exchange occurring at distances of 1-5 m from the contact (Cartwright and Valley, 1991; Park et al., 1999).

Lithium compositions

If there was oxygen isotopic exchange across the Phepane Dome-Bushveld Complex contact, it occurred over distances of < 4 m. Because Li is a fluid-mobile element with a greater diffusivity than most other major elements (Richter et al., 1999), the same samples were measured for their Li concentration and isotopic composition to see if Li exchange had reached farther from the contact. Although the Li data are variable within each rock type, the Li concentrations and isotopic compositions of adjacent rock types exhibit distinct differences.

Lithium concentrations and isotopic compositions of the Bushveld Complex rocks are similar to those of corresponding lithologies worldwide. The Li compositions of the felsic Bushveld Complex rock fall within the range in composition of both A-type granites from China (Li concentrations from 2.8 to 80 ppm, δ^7Li from -1.8 to 6.9‰; Teng et al., 2009) and I-type granites from Greenland (5 to 13 ppm, 0.4 to 6.3‰; Marks et al., 2007). The isotopic composition of the mafic rock is consistent with the average of the deep continental crust (average δ^7Li = 2.5‰; Teng et al., 2008) and measurements of unaltered MORB (1.5 to 5.6‰; Tomascak et al., 2008), however concentrations are higher than unaltered MORB (3-8 ppm, Ryan and Langmuir, 1987) and lower continental crust (average 8 ppm).

The Bushveld Complex mafic rock has up to ten times as much Li as the felsic rock, which is unusual considering that more differentiation is thought to concentrate the moderately incompatible element Li. It implies that the mafic and felsic rock have different sources, which is also suggested by the oxygen isotopic compositions. Lithium isotopic compositions have been shown to remain constant during differentiation (Tomascak et al., 1999; Marks et al., 2007; Teng et al., 2009) and therefore do not support or preclude a different source for the mafic and felsic Bushveld Complex rock.

Lithium compositions of the metasedimentary rocks in the Phepane Dome for the most part fall within the ranges defined by protolith rocks distal from the contact of the Bushveld. The sandstones and quartzites have higher δ^7Li compared to the shales and metapelites, which is consistent with the observation that quartz is usually enriched in ^{7}Li relative to clay minerals (Chan et al., 2006). However, it is difficult to correlate the Li compositions of the unmetamorphosed Lakenvalei Sandstones to the Lakenvalei Quartzite in the Phepane Dome, because there is considerable variability in concentration (2.3 to 13 ppm) and δ^7Li values (12.4 to 21.7‰).

Modeling of isotopic exchange between Phepane Dome and Bushveld Complex

The process of isotopic exchange between the metasedimentary diapir and the surrounding Bushveld magma should occur over the same general timeframe as the process of diapir formation. The diapiric rise of the Phepane Dome occurred due to the heating and cooling of the Transvaal Sedimentary rocks; these are the same processes that control recrystallization and isotopic exchange between magma and metasedimentary rock. Both the Cawthorn and Walraven (1998) and the Gerya et al. (2004) models use a solidus temperature for the Bushveld Complex magma of ~900°C. This is well above the closure temperature for quartz in these rocks (see discussion above). While the closure temperature for Li in these minerals is not known, diffusion of Li has been documented at temperatures from ~350° to 600°C in the contact metamorphic setting of the Tin Mountain pegmatite (Teng et al., 2006a). Thus a duration estimate determined based on diffusion of both O and Li will likely provide a maximum estimate of the time of formation of the Phepane Dome.

Profiles were fit to the measured O and Li compositions using a one-dimensional solution to the mass continuity equation:

$$\frac{\partial C}{\partial t}K_e + v\phi\frac{\partial C}{\partial x} = D_e\frac{\partial^2 C}{\partial x^2} \tag{1}$$

where C is concentration, x is distance from the contact, t is time, v is the Darcy velocity, ϕ is the porosity, D_e is the effective diffusivity, and K_e is the effective partition coefficient. The effective partition coefficient takes into account the porosity (ϕ) of the rocks as well as the fractionation of the elements into the solid or fluid (Cartwright and Valley, 1991):

$$K_e = \frac{\rho_s K_c}{\rho_f}(1-\phi)+\phi \tag{2}$$

where ρ_s and ρ_f are the density of the solid and fluid respectively and K_c is the partition coefficient between the mineral and fluid. Isotopic exchange of O and Li is assumed to occur within an intergranular medium. The effective diffusivity D_e is defined as (Cartwright and Valley, 1991):

$$D_e = \phi D \tau \tag{3}$$

where τ is the tortuosity of the system and D is the diffusivity of the element or isotope in the medium (aqueous fluid or melt).

Values for densities of the rock (ρ_s = 2700 kg/m^2) and melt (ρ_f = 2400 kg/m^2) are taken from estimates for densities of the solid and molten rock in the Gerya et al. (2004) model. The porosity for diffusion through a partial melt (φ =0.01) used in the models was estimated from the abundance of cuspate plagioclase in the Lakenvalei Quartzite as a proxy for the amount of melt. This is likely a minimum constraint and will lead to a calculation of a maximum duration of diffusion. A range of porosities for diffusion through an intergranular aqueous fluid was used, from 10^{-3} to 10^{-5} (e.g. Norton and Knapp, 1977; Bickle and Baker, 1990; Baxter and DePaolo, 2002). Tortuosity is estimated as τ =1 for metamorphic rocks of these porosities (Cartwright and Valley, 1991).

In three of the four traverses, the best-fit solution to the mass continuity equation for Li was found using a model with no advection, only diffusion. The two of these three traverses for which O isotope exchange was also modeled also were fit best by diffusion-only solutions. The modeled profiles were matched to the data to solve for the diffusive distance $\sqrt{D_e t K_e^{-1}}$ and to resolve the duration (t) of a metamorphic event from the diffusive distance. In the West Large-scale traverse, however, an advective component was required to satisfactorily model the Li data (there is no O isotope data for this traverse). In this traverse, the modeled profiles were also matched to the data to solve for the advective distance $z^* = \frac{v\phi t}{K_e}$.

It is recognized that ^{6}Li diffuses faster than ^{7}Li, and this difference in diffusivity is quantified through the empirical term β (Richter et al., 2003), where

$$\frac{D_{^6Li}}{D_{^7Li}} = \left(\frac{m_{^7Li}}{m_{^6Li}}\right)^{\beta} \quad (5)$$

and $D_{x_{Li}}$ and $m_{x_{Li}}$ refer to the diffusivity and mass of the specific (x) isotopes of Li (6 and 7). For condensed material, β is <0.5, with studies finding β= 0.215 for silicate melts, β= 0.12 for aqueous fluid, and β< 0.071 for Li diffusion in water (Richter et al, 2003; Teng et al., 2006, Fritz, 1992, and Penniston-Dorland et al., 2010; and Richter et al., 2006; respectively). To model Li diffusion with differing isotopic diffusivities, the ^{7}Li and ^{6}Li concentrations are modeled separately, with the ratio of D_{Li} for ^{7}Li and ^{6}Li calculated from β. The δ^7Li at each distance from the contact can be calculated from the modeled isotopic concentrations at that distance. In the case of oxygen isotopes, the diffusion is modeled as self diffusion in which the δ^{18}O values are modeled as concentration.

Oxygen Models

The best fit to the O isotope data is shown in Figure 6 and in Table 6. The solution to the model equation for the East Phepane traverse is a characteristic diffusion distance $\sqrt{D_e t K_e^{-1}}$ =1.1 m. The best fit for this model and all models in this study is determined using the statistical χ^2 test (from Bevington and Robinson, 1992). Because the desired result of this model is the maximum duration of diffusion, the greatest possible diffusive distance that can still fit the data is also considered, as this will produce a greater time estimate. The greatest diffusive distance is $\sqrt{D_e t K_e^{-1}}$ =1.4 m (Figure 6a).

Using these model results and estimates from empirical data to calculate D_e and K_e constrains the duration of diffusion (t). For oxygen diffusion through melt, the estimated porosity and a partition coefficient (K_c) for oxygen of 0.55 (Cartwright and Valley, 1992), result in a K_e of 0.62. Partial melting of the Phepane sedimentary rock likely occurred at T~800°C because the felsic melt would have a lower solidus temperature than the mafic magma, and the temperature of the partially melted core of the Phepane Dome was determined to be >720°C (Johnson et al., 2004). Melting of the Phepane rock at these lower temperatures was likely fluid assisted, and therefore the experimentally determined diffusivity of oxygen through rhyolite in the presence of water was used (D=9x10^{-13} m^2/s at ~800°C, Behrens et al., 2007) resulting in a D_e for O diffusion through melt of 9x10^{-15} m^2/s. The resulting estimate for the duration of O isotopic exchange through melt using the best-fit model is 2.6 Myrs, while the maximum time estimate is 4.2 Myrs.

Diffusion may have occurred over part of the exchange history through an aqueous fluid, and the range of time estimates for diffusion through aqueous fluid can also be calculated. Using the diffusivity of oxygen through aqueous fluid (D_O=10^{-8} m^2/s; Bickle and McKenzie, 1987) and the lowest porosity of 10^{-5}, the slowest effective diffusivity through aqueous fluid is calculated for the East Phepane traverse (D_e=10^{-13} m^2/s). The effective partition coefficient utilizes the same K_c, but is larger for solid-fluid partitioning because the density of the fluid is now lower (800 kg/m^2; K_e= 1.86) compared to the density of the melt. These parameters result in a maximum estimate of the duration of exchange through an intergranular aqueous fluid of 1.2 Myrs (lowest porosity, highest $\sqrt{D_e t K_e^{-1}}$). Varying the porosity and the $\sqrt{D_e t K_e^{-1}}$ results in estimates of duration as short as 7 kyrs (Table 6).

While these calculations are informative, since the igneous rock in contact with the quartzite in the East is a felsic rock, it may not provide a true estimate of the cooling history of the mafic Bushveld Complex. For that we need to turn to the west side traverses, in which the igneous rock is mafic.

Since there is no quartz in the mafic Bushveld rock, modeling of the West Small Scale Transect requires the calculation of compositions of fictive quartz in the mafic rock to constrain the extent of across-contact oxygen isotopic exchange with the Lakenvalei Quartzite. The compositions of the fictive quartz are calculated at 900°C, which is the preferred temperature for the mafic magma as discussed above. Modeling was calculated similar to that for the East Phepane traverse, with the best-fit model resulting in a diffusive distance of $\sqrt{D_e t K_e^{-1}}$ =0.9 m, and the maximum diffusive distance is 1.5 m (Figure 6b). Similar values were used for parameters (D_e, K_e) used to calculate time from these results as for the East Phepane. The values for porosity, tortuosity, partition coefficients and diffusion coefficient for Li through aqueous fluid would all be the same across the contact with a mafic melt as they would be for a felsic melt. The one parameter that could potentially be different would be the effective diffusivity for diffusion of Li through mafic magma. We calculate this value using the diffusivity of oxygen through basalt melt at 900°C of 9×10^{-13} m^2/s (Wendlandt, 1991), which combined with porosity and tortuosity produce an effective diffusivity of $D_e = 9 \times 10^{-15}$ m^2/s. For oxygen diffusion through melt, the best fit model results in a time estimate of 1.8 Myrs and the maximum diffusive distance results in a time estimate of 4.9 Myrs. For O diffusion through aqueous fluid, the maximum duration estimate is 1.3 Myrs (lowest porosity, highest $\sqrt{D_e t K_e^{-1}}$). Varying the porosity and the $\sqrt{D_e t K_e^{-1}}$ results in estimates of duration as short as 3 kyrs (Table 6).

As there is evidence for both partial melt and aqueous fluid in the Phepane Dome rocks, the constraint that can be placed on the oxygen isotopic exchange between the Phepane Dome and the Bushveld Complex is a maximum duration of 4.9 Myrs. This maximum time estimate is constrained by the maximum diffusive distance for the West Phepane Large scale traverse using the relatively slow diffusivity of oxygen through melt. This amount of time is consistent with the estimates of both Cawthorn and Walraven (1998) and Gerya et al. (2004).

Lithium models

Since Li is a moderately incompatible and fluid-mobile element, Li concentrations and δ^7Li are also likely to be modified by exchange due to melt- and aqueous fluid-rock interactions at the contact between the Bushveld and the Phepane Dome. The lithium concentrations and δ^7Li values of the various rock types are more variable than the oxygen isotopic compositions. Lithium substitutes readily for Mg in octahedral sites due to their similar ionic radius. Mafic minerals such as amphiboles, pyroxenes, and chlorite may therefore have the highest concentrations of Li in these rocks. While variability in Li concentration is likely due to the processes of diffusion investigated here, some variability is also likely due to varying proportions of these minerals. For this reason, determination of the best-fit model profiles to the data was primarily based on the isotope data.

In the West small-scale traverse there is a distinct jump in δ^7Li and Li concentration over a relatively short distance (1 m) across the contact. The Li concentration of the mafic rock is higher than that in the quartzite (19 ppm vs. 16 ppm), and the isotopic composition of the mafic rock is significantly lower than that of the quartzite (3.4‰ vs. 8.1‰). The results for each rock type moving away from the contact show a more gradational variation in Li concentration and isotopic composition. The dramatic difference at the contact is over such a short distance that it cannot be explained by exchange of Li by either diffusion or advection through an intergranular fluid. One possible explanation is that the two rock types exchanged Li through an intergranular fluid, but the mineral phases in each of the rock types partitioned and fractionated Li differently. Thus, the fluid composition that was in equilibrium with the two rocks would have been the same across the contact, but the two different rock types would have different bulk rock isotopic compositions and concentrations due to fractionation/partitioning between the fluid and the different mineral assemblages. Differences in δ^7Li and Li concentration between samples across the other contacts are consistent with this hypothesis (e.g., the mafic rocks adjacent to the contact all have consistently higher concentrations of Li and have lower δ^7Li compared to the quartzite). To account for differences in fractionation and partitioning in the models, the Li concentration and δ^7Li of the modeled igneous rocks were adjusted for fractionation and partitioning by a constant amount, defined by the difference between the closest samples of quartzite and each of the igneous rocks. In the models for the west-side traverses, the model mafic rock compositions were adjusted for fractionation and partitioning: $\Delta^7 Li_{sed-mafic}$=4.7‰, $D^{Li}_{sed/mafic}$ =0.6 where $\Delta^7 Li_{sed-mafic} = \delta^7 Li_{sed} - \delta^7 Li_{mafic}$ and $D^{Li}_{sed/mafic} = \frac{C^{Li}_{sed}}{C^{Li}_{mafic}}$. In the model for the east-side traverse, the model felsic rock compositions were adjusted for partitioning by $D^{Li}_{sed/felsic}$=1.6. However, the δ^7Li of the closest samples on either side of the contact from the east side (the East ’07 traverse) are within uncertainty of having the same δ^7Li value (+12.8‰ and +12.1‰), so no adjustment was made for isotopic fractionation on the east traverses.

While the data from both traverses on the east and the small-scale traverse on the west can be explained by diffusion of Li through an intergranular fluid across the contact, the west large-scale traverse is best explained by a model including diffusion along with a minor advective component (~20 m advective distance in the direction of the mafic rock).

Diffusion profiles were fit to all four traverses (Figure 8, Table 6). Initial Li isotopic compositions and concentrations were taken from the average compositions of samples farthest from the contact. The best-fit model solutions for the diffusive distances range from $\sqrt{D_e t K_e^{-1}}$ = 2.4 to 10.6 m. The β value used in these models is 0.17, which is the value that best fits the data. This value is consistent with previously determined β values. It is greater than the β values used by Teng et al. (2006) for Li diffusion through a magmatic fluid (0.12 to 0.15), but less than the β value determined by Richter et al. (2003) for Li diffusion through melt (0.215).

The diffusivities of Li at high temperatures through an intergranular melt or aqueous fluid are not well constrained. The greater diffusive distances for Li compared to those for O is predicted by experimental data, which suggests that the diffusivity of Li can be up to 3 orders of magnitude greater than major elements (Richter et al., 2003). The data provide the opportunity to evaluate the relative diffusivity of O and Li. In order to evaluate the relative diffusivities, the partition coefficient for Li must be characterized. The same density parameters of the Phepane Dome and Bushveld Complex rocks are used in the calculation of the effective partition coefficient, but the solid-melt partition coefficient (K_c) of Li must be quantified. A K_c of 0.1 is used (Brenan et al., 1998) with the caveat that it is for cpx-melt and not the rock compositions or minerals of this transect. The effective partition coefficient solid-melt partition coefficient (K_c) is calculated to be 0.12, compared to an effective partition coefficient for oxygen of 0.62. Assuming that the time for diffusion of O and Li was the same, this value can be used with the effective partition coefficient for rock-melt for O described above and the different diffusive distances along the west small-scale contact to calculate the relative diffusivities of Li and O. Since the diffusive distance for Li in the West small scale traverse is 10 times greater than for O (10.6 compared to 0.91), the diffusivity of Li scales as the square of the ratio of the diffusive distances (100) multiplied by the ratio of the two partition coefficients, resulting in a diffusivity of Li that is ~20 times greater than the diffusivity of O.

Implications

Evidence from petrographic and cathodoluminescence analysis in the Phepane Dome indicates that the quartzites recrystallized and experienced partial melting at the peak of metamorphism. The dihedral angle analysis of Lakenvalei quartzite samples from both sides of the Phepane Dome indicates the presence of a low-angle peak at ~40-50°. This range of angles is consistent with partial melting of the Lakenvalei at the grain-scale and suggests that partial melt in the Lakenvalei was connected along grain boundaries, allowing for across-contact diffusive exchange. Cathodoluminescence imaging of the quartzite indicates three different stages of metamorphism and interaction with fluids: an early high-temperature recrystallization of quartz indicated by bright blue luminescing quartz cores (in contrast to the dark red luminescence of the protolith sandstone); a later, lower-temperature further recrystallization of quartz indicated by a darker blue luminescence on the edges of grains, associated with fluid inclusions; and a volumetrically minor late-stage crystallization of quartz along fractures that cross-cut earlier formed quartz and feldspars.

There is a significant difference in the oxygen isotopic composition of the three different rock types analyzed for this study. The change in isotopic composition across the contact between quartzite and igneous rock occurs over distances of < ~4 m. The two samples closest to the contact in each of the two traverses show evidence for isotopic exchange between the two reservoirs. One-dimensional solutions to the mass continuity equation show that the isotopic variations in both traverses can be explained by diffusion of oxygen across the boundary between the two disparate rock types. Estimates of the parameters involved in the modeling suggest that this exchange occurred for less than 5 Myrs, which is consistent with the amount of time predicted by both models (Cawthorn and Walraven, 1998; Gerya et al., 2004) for the crystallization of the Bushveld and formation of the Phepane Dome. This result is also consistent with the results of Letts et al. (2009) which estimated the total time of cooling of the Bushveld based on paleomagnetic measurements to be a minimum of ~1.4 million years. At a minimum, the time recorded by the diffusion profile represents exchange between the diapir and its surrounding igneous rock after diapiric rise. It is possible that the time may also encompass an earlier part of the exchange between diapir and the Bushveld during its ascent, however, the data do not permit speculation about this.

The igneous rocks of the Bushveld Complex have elevated $\delta^{18}O$ relative to mantle-derived rocks (Schiffries and Rye, 1989; Harris et al., 2005). Some of the igneous rocks of the Bushveld show signs of isotopic alteration, for example surrounding hydrothermal veins (Schiffries and Rye, 1990), however the isotopic evidence from mineral pairs suggest that most of the igneous rocks record magmatic isotopic compositions (Harris et al., 2005) with little evidence for exchange with local country rocks. Samples of the same quartzite units that have been analyzed in this study (Lakenvalei and Magaliesburg) from the northeastern edge of the Bushveld Complex have $\delta^{18}O$ values that show no change in $\delta^{18}O$ related to the distance from the contact (Harris et al., 2003), and are interpreted to result from infiltration of fluids derived from dehydration of dehydrating metasedimentary rocks. Elsewhere in the eastern lobe of the Bushveld, at an external contact with the Steenkampsberg Quartzite, Schiffries and Rye (1990) documented a decrease in $\delta^{18}O$ in the quartzite approaching the contact with the igneous rock over a distance of at least 2 km. This isotopic variation was attributed to pervasive fluid infiltration within the quartzite by externally-derived fluids (either from other country rocks or from the Bushveld). The O isotopic compositions of calcareous country rocks and xenoliths in the Bushveld also demonstrate a decrease in $\delta^{18}O$ approaching the Bushveld (Buick et al., 2000) which is interpreted as the result of interaction with fluids derived from adjacent dehydrating country rocks.

There are relatively few contact aureoles in which there is documented isotopic alteration consistent with diffusion alone across the contact between igneous rock and the wall rock (without requiring significant fluid infiltration). One example is adjacent to a granite body in the Adirondacks, where oxygen isotope alteration is restricted to relatively small scales, < ~5 m (Cartwright and Valley, 1991). In another example, at Quérigut in the Eastern Pyrenees of France, contacts between the granite and internal septa exhibited exchange dominated by diffusion on a scale of ~2 m (Durand et al., 2006). In this locality traverses across an outer contact of the same granite with carbonate country rock exhibited extensive oxygen isotopic alteration, consistent with fluid infiltration.

The results from the Phepane Dome suggest that while heat transfer caused complete recrystallization and partial melting of the metasedimentary rock, relatively minimal chemical exchange occurred during interaction between the Phepane Dome and the surrounding Bushveld magma. This limited exchange is in contrast to the large-scale isotopic variability observed in country rocks surrounding the Bushveld which is attributed to advection by fluids during high temperature metamorphism. These results suggest that the Phepane Dome experienced relatively limited fluid infiltration .

The lithium concentrations and δ^7Li values of the various rock types are more variable than the oxygen isotopic compositions. There is some systematic variation in Li concentration and isotopic composition along the profiles that is due to the processes of diffusion investigated here, however some variability in Li concentration is likely due to varying proportions of Li-rich minerals. Very small-scale "jumps" in concentration and isotopic composition across lithologic contacts are attributed to partitioning and fractionation of Li between the different minerals existing in each rock type and the coexisting melt or aqueous fluid. Taking all these factors into consideration, the modeling profiles suggest diffusion of Li over distances of < 60 m. The calculated diffusive distance for Li is one order of magnitude greater than for O in the same samples. Correcting for the different partition coefficients of O and Li results in a Li diffusivity that is about 20 times greater than the associated O diffusivity. This supports the experimental evidence that suggests that Li has a greater diffusivity than other major elements.

Acknowledgements.

We thank the Geological Society of America for a student research grant awarded to RI. We thank Mike Spicuzza and John Valley for assistance with oxygen isotope analysis at UW-Madison and Tim Mock and Steve Shirey for assistance with lithium isotope analysis at Carnegie. We thank Ethan Baxter for conversations about diffusion modeling and John Valley for comments on an early draft of this manuscript. Chris Harris and Taras Gerya are thanked for their constructive reviews, and Dionysis Foustoukos is thanked for his patient handling of the manuscript. We thank Sorena Sorensen for use of the CL instrumentation at the National

Museum of Natural History. Thanks to Phil Piccoli, Richard Ash, and Igor Puchtel for assistance with the EPMA, ICP-MS, and the clean lab at Maryland, respectively. Boz Wing, Roberta Rudnick, and James Farquhar are thanked for fruitful discussions. Boz and Tim Johnson are thanked for help with fieldwork, and we thank Paul Nex and Judith Kinnaird for help with field logistics. We acknowledge the support of the Maryland NanoCenter and its NISPLab.

This is a preprint, the final version is subject to change, of the American Mineralogist (MSA)
Cite as Authors (Year) Title. American Mineralogist, in press.
(DOI will not work until issue is live.) DOI: http://dx.doi.org/10.2138/am-2015-5196

References

Baumgartner L.P., and Valley J.W. (2001) Stable Isotope Transport and contact Metamorphic Fluid Flow. In Valley J.W. and Cole D.R. (eds.) Stable Isotope Geochemistry. Reviews In Mineralogy and Geochemistry. 43. 415-468.

Baxter, E.F., and D.J. DePaolo (2002) Field measurement of high temperature bulk reaction rates II: Interpretation of results from a field site near Simplon Pass, Switzerland. American Journal of Science. 304. 465-316.

Behrens, H., Zhang, Y., Leschik, M., Wiedenbeck, M., Heide, G., and Frischat, G.H. (2007) Molecular H_2O as a carrier for oxygen diffusion in hydrous silicate melts. Earth and Planetary Science Letters. 254. 69-76.

Bevington, P.R., and Robinson, D.K. (1992) Data reduction and error analysis for the physical sciences. The McGraw-Hill Companies, Inc. New York City, 219 p.

Bickle, M.J., and Baker, J. (1990) Advective-diffusive transport of isotopic fronts: an example from Naxos, Greece. Earth and Planetary Science Letters. 97. 78-93.

Bickle, M.J., and McKenzie, D. (1987) The transport of heat and matter by fluids during metamorphism. Contributions to Mineralogy and Petrology. 95. 384-392.

Boggs Jr., S., Kwon, Y.-I., Goles, G.G., Rusk, B.G., Krinsley, D., and Seyedolali, A. (2002) Is quartz cathodoluminscence color a reliable provenance tool? A quantitative examination. Journal of Sedimentary Research. 72. 408-415.

Brenan, J.M., Ryerson, F.J., and Shaw, H.F. (1998) The role of aqueous fluids in the slab-to-mantle transfer of boron, beryllium, and lithium during subduction. Geochimica et Cosmochimica Acta. 62. 3337-3347.

Buick, I.S., Gibson, R.L., Cartwright, I., Maas, R., Wallmach, T., and Uken, R. (2000) Fluid flow in metacarbonates associated with emplacement of the Bushveld Complex, South Africa. Journal of Geochemical Exploration. 69-70. 391-395.

Buick, I.S., Maas, R., and Gibson, R. (2001) Precise U-Pb titanite age constraints on the emplacement of the Bushveld Complex, South Africa. Journal of the Geological Society (London, U.K.). 158. 3-6.

Cartwright, I., and Valley, J.W. (1991) Steep oxygen-isotope gradients at marble-metagranite contacts in the northwestern Adirondack Mountains, New York, USA: products of fluid-hosted diffusion. Earth and Planetary Science Letters. 107. 148-163

Cawthorn, R.G., and Walraven, F. (1998) Emplacement and Crystallization Time for the Bushveld Complex. Journal of Petrology. 39. 1669-1687.

Cawthorn, R.G. (1999) The platinum and palladium resources of the Bushveld Complex. South African Journal of Science. 95. 481-489.

Chan, L.H., Leeman, W.P., and Plank, T. (2006) Lithium isotopic composition of marine sediments. Geochemistry Geophysics and Geosystems. 7. Q06005.

Cherniak, D.J. (2000) Pb diffusion in rutile: Contributions to Mineralogy and Petrology. 139. 198–207.

Cherniak, D.J., and Watson, E.B. (2000) Pb diffusion in zircon: Chemical Geology. 172. 5–24.

Clarke, B.M., Uken, R., Watkeys, M.K., and Reinhardt, J. (2005) Folding of the Rustenburg Layered Suite adjacent to the Steelpoort pericline: implications for syn-Bushveld tectonism in the Eastern Bushveld Complex. South African Journal of Geology. 108. 397-412.

Clayton, R.N., and Kiefer, S.W. (1991) Oxygen isotope thermometer calibrations. In Taylor, Jr., H.P., O'Neil, J.R., and I.R. Kaplan, (eds.) Stable Isotope Geochemistry: A Tribute to Samuel Epstein. Special Publication. 3. 3-10.

Dodson, M.H. (1973) Closure temperature in cooling geochronological and petrological systems. Contributions to Mineralogy and Petrology. 40. 259–274.

Durand, C., Boulvais, P., Marquer, D., and Rossy, M. (2006) Stable isotope transfer in open and closed system across chemically contrasted boundaries: metacarbonate-granitoid contacts in the Quérigut magmatic complex (Eastern Pyrenees, France). Journal of the Geological Society, London. 163, 827-836.

Eiler, J.M. (2001) Oxygen isotope variations of basaltic lavas and upper mantle rocks. In Valley, J.W., and Cole, D.R., (eds.) Stable Isotope Geochemistry. Reviews in Mineralogy. 43. 319-364.

Eriksson, P.G., Altermann W., Catuneanu, O., van der Merwe, R., and Bumby, A.J. (2001) Major influences on the evolution of the 2.67-2.1 Ga Transvaal basin, Kaapvaal craton. Sedimentary Geology Special Issue. 241. 205-231.

Fourie, D.S., and Harris, C. (2011) O-isotope study of the Bushveld Complex granites and granophyres: Constraints on source composition, and assimilation. Journal of Petrology, 52, 2221-2242.

Fritz, S.J. (1992) Measuring the ratio of aqueous diffusion-coefficients between ^{7}LiCl and ^{6}LiCl by osmometry. Geochimica et Cosmochimica Acta. 56. 3781-3789.

Gerya, T.V., and Yuen, D.A. (2003) Rayleigh-Taylor instabilities from hydration and melting propel ‘cold plumes’ at subduction zones. Earth and Planetary Science Letters 212. 47-62.

Gerya, T.V., Uken R, Reinhardt J, Watkeys M.K., Maresch W.V., and Clarke, B.M. (2003) Cold fingers in a hot magma: Numerical modeling of country-rock diapirs in the Bushveld Complex, South Africa. Geology. 39. 753-756.

Gerya, T.V., Uken, R., Reinhardt, J., Watkeys, M.K., Maresch, W.V., and Clarke, B.M. (2004) “Cold” diapirs triggered by intrusion of the Bushveld Complex: Insight from two-dimensional numerical modeling. Geological Society of America Special Paper 380.

Giletti, B.J. (1986) Diffusion effects on oxygen isotopic temperatures of slowly cooled igneous and metamorphic rocks. Earth and Planetary Science Letters. 77. 218-228.

Giletti, B.J. and Yund, R.A. (1984) Oxygen diffusion in quartz. Journal of Geophysical Research 89, B6. 4039-4046.

Götze, J., Plotze, M., and Habermann, D. (2001) Origin, spectral characteristics and practical applications of the cathodoluminescence (CL) of quartz- a review. Mineralogy and Petrology. 71. 225-250.

Hall, P.S., and Kincaid, C. (2001) Diapiric Flow at Subduction Zones: A Recipe for Rapid Transport. Science. 292. 2472-2475.

Hannah, J.L., Bekker, A., Stein, H.J., Markey, R.J., and Holland, H. (2004) Primitive Os and 2316 Ma age for marine shale: implications for Paleoproterozoic glacial events and the rise of atmospheric oxygen. Earth and Planetary Science Letters. 225. 43-52.

Harris, N., McMillan, A., Holness, M., Uken, R., Watkeys, M., Rogers, N., and Fallick, A. (2003) Melt Generation and Fluid Flow in the Thermal Aureole of the Bushveld Complex. Journal of Petrology. 44. 1031-1054.

Harris, C., Pronost, J.J.M., Ashwal, L.D., and Cawthorn, R.G. (2005) Oxygen and Hydrogen Isotope Stratigraphy of the Rustenburg Layered Suite, Bushveld Complex: Constraints on Crustal Contamination. Journal of Petrology. 46. 575-601.

Hill, M., Barker, F., Hunter, D., and R. Knight (1996) Geochemical Characteristics and Origin of the Lebowa Granite Suite, Bushveld Complex. International Geology Review. 38. 195-227.

Holness, M.B. (1998) Contrasting rock permeability in the aureole of the Ballachulish igneous complex, Scottish Highlands: the influence of surface energy? Contributions to Mineralogy and Petrology. 131. 86-94.

Holness, M.B. (2006) Melt-solid dihedral angles of common minerals in natural rocks. Journal of Petrology. 47. 791-800.

Ito, E., White, W.M., and Gopel, C. (1987) The O, Sr, Nd, and Pb isotope geochemistry of MORB. Chemical Geology. 62. 157-176.

Johnson, T.E., Gibson, R.L., Brown, M., Buick, I.S., and Cartwright, I. (2003) Partial melting of metapelitic rocks beneath the Bushveld Complex, South Africa. Journal of Petrology. 44. 789-813.

Johnson, T., Brown, M., Gibson, R., and Wing, B. (2004) Spinel-cordierite symplectites replacing andalusite: evidence for melt-assisted diapirism in the Bushveld Complex, South Africa. Journal of Metamorphic Geology. 22. 529-545.

Kinnaird, J.A., Hutchinson, D., Schurmann, L., Nex, P.A.M., and de Lange, R. (2005) Petrology and mineralization of the southern Platreef: northern limb of the Bushveld Complex, South Africa. Mineralium Deposita. 40. 576-597.

Letts, S., Torsvik, T.H., Webb, S.J., and Ashwal, L.D. (2009) Palaeomagnetism of the 2054 Ma Bushveld Complex (South Africa): implications for emplacement and cooling. Geophysical Journal International. 179. 850-872.

Marks, M.A.W., Rudnick, R.L., McCammon, C., Vennemann, T., and Markl, G. (2007) Arrested kinetic Li isotope fractionation at the margin of the Ilimaussaq complex, South Greenland: Evidence for open-system processes during the final cooling of per-alkaline igneous rocks. Chemical Geology. 246. 207-230.

Molyneux, T.G., and Klinkert, P.S. (1978) A structural interpretation of part of the eastern mafic lobe of the Bushveld Complex and its surrounds. Transactions of the Geological Society of South Africa. 81. 359-368.

Moriguti, T., and Nakamura, E. (1998) High-yield lithium separation and the precise isotopic analysis for natural rock and aqueous samples. Chemical Geology. 145. 91-104.

Nomade, S., Renne, P.R., and Merkle, R.K.W. (2004) 40Ar/39Ar constraints on ore deposition and cooling of the Bushveld Complex, South Africa. Journal of the Geological Society London. 161. 411-420.

Norton, D., and Knapp, R. (1977) Transport phenomena in hydrothermal systems: The nature of porosity. American Journal of Science. 277. 913-936.

Park, W.R., Ripley, E.M., Severson, M., and Hauck, S. (1999) Stable isotopic studies of mafic sills and Proterozoic metasedimentary rocks located beneath the Duluth Complex, Minnesota. Geochimica et Cosmochimica Acta. 6. 657-674.

Penniston-Dorland, S. (2001) Illumination of vein quartz textures in a porphyry copper ore deposit using scanned cathodoluminescence: Grasberg Igneous Complex, Irian Jaya, Indonesia. American Mineralogist. 86. 652-666.

Penniston-Dorland, S.C., Sorensen, S.S., Ash, R.D., and Khadke, S.V. (2010) Lithium isotopes as a tracer of fluids in a subduction zone mélange: Franciscan Complex, CA. Earth and Planetary Science Letters. 292. 181-190.

Richter, F.M., Liang, Y., and Davis, A.M. (1999) Isotope fractionation by diffusion in molten oxides. Geochimica et Cosmochimica Acta. 63. 2853-2861.

Richter, F.M., Davis, A.M., DePaolo, D.M., and Watson, E.B. (2003) Isotope fractionation by chemical diffusion between molten basalt and rhyolite. Geochimica et Cosmochimica Acta. 67. 3905-3923.

Richter, F.M., Mendybaev, R.A., Christensen, J.N., Hutcheon, I.D., Williams, R.W., Sturchio, N.C., and Beloso Jr., A.D., 2006. Kinetic isotopic fractionation during diffusion of ionic species in water. Geochimica et Cosmochimica Acta. 70. 277-289.

Rudnick, R.L., Tomascak, P.B., Njo, H.B., and Gardner, R.L. (2004) Extreme lithium isotopic fractionation during continental weathering revealed in saprolites from South Carolina. Chemical Geology. 212. 45-57.

Rusk, B.G., Lowers, H.A., and Reed, M.H. (2008) Trace elements in hydrothermal quartz: Relationships to cathodoluminescent textures and insights into vein formation. Geology. 36. 547-550.

Ryan, J.G., and Langmuir, C.H. (1987) The systematics of lithium abundances in young volcanic rocks. Geochimica et Cosmochimica Acta. 51. 1727-1741.

Schiffries, C.M., and Rye, D.M. (1989) Stable isotopic systematics of the Bushveld Complex: I. Constraints on magmatic processes in layered intrusions. American Journal of Science. 289. 841-873.

Schiffries, C.M., and Rye, D.M. (1990) Stable isotopic systematics of the Bushveld Complex: II. Constraints on hydrothermal processes in layered intrusions. American Journal of Science. 290. 209-245.

Schweitzer, J.K., Hatton, C.J., and de Waal, S.A. (1997) Link between the granitic and volcanic rocks of the Bushveld Complex, South Africa. Journal of African Earth Sciences. 24. 95-104.

Scoates, J.S., and Friedman, R.M. (2008) Precise age of the platiniferous Merensky Reef, Bushveld Complex, South Africa, by the U-Pb zircon chemical abrasion ID-TIMS technique. Economic Geology. 103. 465-471.

Shieh, Y.N., and Taylor, Jr., H.P. (1969) Oxygen and carbon isotope studies of contact metamorphism of carbonate rocks. Journal of Petrology. 10. 307-331.

Sprunt, E., Dengler, L., and Sloan, D. (1978) Effects of metamorphism on quartz cathodoluminescence. Geology. 6. 305-308.

Teng, F.Z., McDonough, W.F., Rudnick, R.L., Dalpe, C., Tomascak, P.B., Chappell, B.W., and Gao, S. (2004) Lithium isotopic composition and concentration of the upper continental crust. Geochimica et Cosmochimica Acta. 68. 4167-4178

Teng, F.Z., McDonough, W.F., Rudnick, R.L., and Walker, R.J. (2006a) Diffusion-driven extreme lithium isotopic fractionation in country rocks of the Tin Mountain pegmatite. Earth and Planetary Science Letters. 243. 701-710.

Teng, F.Z., McDonough, W.F., Rudnick, R.L., Walker, R. J., and Sirbescu, M.C. (2006b) Lithium isotopic systematics of granites and pegmatites from the Black Hills, South Dakota. American Mineralogist. 91. 1488-1498.

Teng, F.-Z., Rudnick, R.L., McDonough, W.F., Gao, S., Tomascak, P.B., and Liu, Y. (2008) Lithium isotopic composition and concentration of the deep continental crust. Chemical Geology. 255. 47-59.

Teng, F.-Z., Rudnick, R.L., McDonough, W.F., and Wu, F.-Y. (2009) Lithium isotopic systematics of A-type granites and their mafic enclaves: Further constraints on the Li isotopic composition of the continental crust. Chemical Geology. 262. 370-379.

Tomascak, P.B., Tera, F., Helz, R.T., and Walker, R.J. (1999) The absence of lithium isotope fractionation during basalt differentiation: New measurements by multicollector sector ICP-MS. Geochimica et Cosmochimica Acta. 63. 907-910.

Tomascak, P.B., Langmuir, C.H., le Roux, P.J., and Shirey, S.B. (2008) Lithium isotopes in global mid-ocean ridge basalts. Geochimica et Cosmochimica Acta. 72. 1626-1637.

Uken, R., and Watkeys, M.K., 1997. Diapirism initiated by the Bushveld Complex, South Africa. Geology. 25. 723-726.

Valley, J.W., Kitchen, N., Kohn, M.J., Niendorf, C.R., and Spicuzza, M.J. (1995) UWG-2, a garnet standard for oxygen isotopic ratios: Strategies for high precision and accuracy with laser heating. Geochimica et Cosmochimica Acta. 59. 5223-5231.

Valley, J.W., and Graham, C.M. (1996) Ion microprobe analysis of oxygen isotope ratios in quartz from Skye granite: Healed micro-cracks, fluid flow, and hydrothermal exchange. Contributions to Mineralogy and Petrology 124. 225-234.

Vernon, R.H. (1968) Microstructures of high-grade metamorphic rocks at Broken Hill Australia. Journal of Petrology. 9. 1-22.

Walraven, F., Armstrong, R.A., and Kruger, F.J. (1990) A chronostratigraphic framework for the north-central Kaapvaal craton, the Bushveld Complex and Vredefort structure. Tectonophysics. 171. 23-48.

Watson, E.B, and Baxter, E.F. (2007) Diffusion in solid Earth systems. Earth Planet. Sci. Lett. 253. 307-327.

Wendlandt, R.W. (1991) Oxygen diffusion in basalt and andesite melts: Experimental results of chemical versus tracer diffusion. Contributions to Mineralogy and Petrology. 108. 463-471.

1030 **Table 1**. Sample locations

Sample	Lithology	Latitude, Longitude	Distance from contact (m)*
		East Phepane 06 Transect	
P06-1	felsic rock	S 24º 29.876’ E 029º 52.833’	
P06-2	felsic rock	S 24º 29.882’ E 029º 52.819’	
P06-3	felsic rock	S 24º 29.886’ E 029º 52.813’	
P06-4	felsic rock	S 24º 29.887’ E 029º 52.813’	
P06-5	felsic rock	S 24º 29.900’ E 029º 52.805’	
P06-6	felsic rock	S 24º 29.897’ E 029º 52.808’	
P06-7	felsic rock	S 24º 29.911’ E 029º 52.794’	23.6 E
P06-8	felsic rock	S 24º 29.909’ E 029º 52.795’	27.9 E
P06-9	felsic rock	S 24º 29.917’ E 029º 52.795’	13.5 E
P06-10	felsic rock	S 24º 29.922’ E 029º 52.794’	8.6 E
P06-11	felsic rock	S 24º 29.921’ E 029º 52.795’	5.0 E
P06-12	felsic rock	S 24º 29.922’ E 029º 52.795’	3.7 E
P06-13	felsic rock	S 24º 29.925’ E 029º 52.792’	1.5 E
P06-14	felsic rock	S 24º 29.919’ E 029º 52.783’	4.3 E
P06-15	quartzite		2.8 W
P06-16	quartzite		7.6 W
P06-17	quartzite		8.6 W
P06-18	quartzite		9.6 W
P06-19	quartzite		13.3 W
P06-20	metapelite	S 24º 29.960’ E 029º 52.783’	
		West Phepane Large Transect	
P07-1	quartzite	S 24º 30.860’ E 029º 51.076’	
P07-2	metapelite	S 24º 29.868’ E 029º 51.090’	
P07-3	quartzite	S 24º 29.883’ E 029º 51.077’	
P07-4	quartzite	S 24º 29.887’ E 029º 51.078’	
P07-5	metapelite	S 24º 29.903’ E 029º 51.074’	
P07-6	mafic rock	S 24º 29.900’ E 029º 51.035’	
P07-7	mafic rock	S 24º 29.896’ E 029º 51.026’	
P07-8	mafic rock	S 24º 29.890’ E 029º 51.011’	
P07-9	mafic rock	S 24º 29.892’ E 029º 51.002’	
P07-10	mafic rock	S 24º 29.887’ E 029º 51.001’	
P07-11	mafic rock	S 24º 29.880’ E 029º 50.971’	
P07-12	mafic rock	S 24º 29.800’ E 029º 50.909’	
P07-13	mafic rock	S 24º 29.810’ E 029º 50.907’	
P07-14	quartzite	S 24º 29.845’ E 029º 51.058’	
P07-15	mafic rock	S 24º 29.872’ E 029º 51.046’	
P07-16	metapelite	S 24º 29.849’ E 029º 51.088’	
P07-17	quartzite	S 24º 29.861’ E 029º 51.052’	
P07-18	metapelite	S 24º 29.868’ E 029º 51.103’	
P07-19	calcsilicate	S 24º 29.861’ E 029º 51.114’	
P07-20	metapelite	S 24º 29.875’ E 029º 51.125’	
P07-21	quartzite	S 24º 29.867’ E 029º 51.140’	
P07-22	quartzite	S 24º 29.856’ E 029º 51.160’	

Table 1. Sample locations (cont.)

Sample	Lithology	Latitude, Longitude	Distance from contact (m)*
West Phepane Large Transect			
P07-23	metapelite	S 24º 29.864’ E 029º 51.198’	
P07-24	metapelite	S 24º 29.886’ E 029º 51.220’	
P07-25	quartzite	S 24º 29.891’ E 029º 51.263’	
West Phepane Small Transect			
P07-26	quartzite	S 24º 30.423’ E 029º 51.090’	
P07-27	metapelite	S 24º 29.415’ E 029º 51.109’	
P07-28	quartzite	S 24º 29.424’ E 029º 51.094’	
P07-29	quartzite	S 24º 29.433’ E 029º 51.077’	
P07-30	quartzite	S 24º 29.422’ E 029º 51.065’	
P07-31	mafic rock	S 24º 29.424’ E 029º 51.064’	9.0 W
P07-32	mafic rock	S 24º 29.423’ E 029º 51.053’	14.0 W
P07-33	mafic rock	S 24º 29.414’ E 029º 51.048’	23.2 W
P07-34	mafic rock	S 24º 29.427’ E 029º 51.045’	32.6 W
East Phepane 07 Transect			
P07-49	felsic rock	S 24º 29.731’ E 029º 52.621’	
P07-50	quartzite	S 24º 29.753’ E 029º 52.582’	0.2 W
P07-51	quartzite	S 24º 29.753’ E 029º 52.582’	4.3 W
P07-52	felsic rock	S 24º 29.753’ E 029º 52.582’	9.3 E
P07-53	felsic rock	S 24º 29.753’ E 029º 52.582’	5.2 E
P07-54	metapelite	S 24º 29.786’ E 029º 52.551’	
P07-55	metapelite	S 24º 29.757’ E 029º 52.581’	
P07-56	metapelite	S 24º 29.763’ E 029º 52.564’	
P07-57	quartzite	S 24º 29.799’ E 029º 52.502’	
P07-58	felsic rock	S 24º 29.748’ E 029º 52.599’	
P07-59	felsic rock	S 24º 29.738’ E 029º 52.602’	
Sedimentary rocks			
LV2	sandstone	S 25º 01.335’ E 030º 13.485’	
LV3	sandstone	S 25º 02.437’ E 030º 13.461’	
LV4	sandstone	S 25º 21.315’ E 030º 10.240’	
LV6	sandstone	S 24º 56.978’ E 030º 13.395’	
VT1a	shale	S 25º 15.170’ E 030º 15.654’	

* Distance measured using steel measuring tape oriented perpendicular to the contact.
W=distance on the west side of the contact, E=distance on the east side of the contact

Table 2. Mineral modes (volume percentage) of representative rock types

Sample	P06-19	P07-28	P06-2	P07-32	P07-6
Type	Lakenvalei Quartzite	Lakenvalei Quartzite	Felsic Rock	Mafic Rock	Mafic Rock
	East	West	East	West	West
Quartz	83.0	87.3	20.9	8.55	0.56
K-feldspar	8.97	8.89	31.8	1.64	0.17
Plagioclase	5.30	3.39	32.2	78.7	64.5
Hornblende	0	0	13.3	7.20	23.9
Clinopyroxene	0	0	0	0.68	3.77
Orthopyroxene	0	0	0	0	5.57
Muscovite	2.56	0.38	0	0.05	0.17
Biotite	0	0	1.4	tr	0
Chlorite	0.19	0.05	0	2.00	1.16
Calcite	0	0.09	0	0.59	0
Zircon	tr*	tr	tr	tr	0
Apatite	tr	tr	0.05	0.55	0
Monazite	tr	0	0.05	0	0
Ilmenite	0	0	0.05	tr	0.13
Magnetite	0	0	0.14	0	tr
Titanite	0	0	0	tr	0
Rutile	0	tr	tr	0	0
Total points	2152	2126	2174	2200	2335

* tr = trace amount, <0.05%

Table 3. Plagioclase major element compositions (wt.%)

Sample	P07-32	P07-32	P07-32	P07-32	P07-32	P07-6	P07-6
SiO_2	51.80	51.55	50.81	50.57	52.53	49.52	50.15
TiO_2	0.00	0.01	0.00	0.00	0.00	0.00	0.00
Al_2O_3	31.17	31.46	30.86	30.67	29.34	31.95	31.59
FeO	0.08	0.11	0.08	0.01	0.07	0.08	0.06
MnO	0.00	0.01	0.00	0.00	0.02	0.01	0.00
MgO	0.02	0.04	0.01	0.04	0.00	0.00	0.00
CaO	13.27	13.58	14.60	13.27	12.95	16.03	15.50
Na_2O	3.83	3.69	3.73	4.18	3.92	3.03	3.33
K_2O	0.11	0.20	0.10	0.08	1.39	0.10	0.09
Total	100.3	100.6	100.2	98.81	100.2	100.7	100.7
X_{An}	0.65	0.66	0.68	0.63	0.60	0.72	0.74
X_{Ab}	0.34	0.33	0.32	0.36	0.33	0.28	0.25
X_{Or}	0.01	0.01	0.00	0.00	0.08	0.00	0.01

Table 4. Oxygen Isotopic Compositions

Sample	Rock Type	Distance (m)[§]	$\delta^{18}O_{qtz}$ (‰)	$\delta^{18}O_{pl}$ (‰)	$\delta^{18}O_{wr}$ (‰)
East Phepane 06 Transect					
P06-1	Felsic rock	108	6.93		
P06-2	Felsic rock	89	7.92		
P06-6	Felsic rock	58	7.09		
P06-8	Felsic rock	30	7.37		
P06-9	Felsic rock	17	7.33		
P06-14	Felsic rock	4.8	6.90		
P06-13	Felsic rock	2.1	7.80		
P06-15	Lakenvalei Quartzite	2.4	10.85		
			11.05*		
P06-16	Lakenvalei Quartzite	7.1	11.34		
P06-18	Lakenvalei Quartzite	9.0	11.27		
			11.41*		
P06-19	Lakenvalei Quartzite	12	11.21		
West Phepane Small Scale Transect					
P07-34	Mafic rock	33		8.02	6.60
					7.05*
P07-33a	Mafic rock	26		8.04	7.39
P07-33b	Mafic rock	26			7.39*
P07-32	Mafic rock	19		7.95	7.90
				7.89†	8.08*
P07-31	Mafic rock	0.8		8.59	8.27
				8.59*	8.12*
				8.54†	
P07-30	Lakenvalei Quartzite	0.6	10.59		
			10.47*		
			10.57†		
P07-26	Lakenvalei Quartzite	42	11.05		
			10.83*		
P07-28	Lakenvalei Quartzite	51	11.06		
			11.08*		
			11.30†		
			11.09†*		

[§] Measured distances corrected for dip of contact and for variations in elevation
* Same sample aliquot measured again
† Different aliquot of same sample

Table 5. Lithium Isotope Compositions and Concentrations

Sample	Rock Type*	Distance (m)[§]	δ^7Li (‰)	Li (ppm)
East Phepane 06 and 07 Transects				
P06-1	Felsic rock (2)	108	5.7	2.8
P06-2	Felsic rock (2)	89	8.2	3.3
P06-3	Felsic rock	79	4.7	4.4
P06-6	Felsic rock	58	8.0	9.1
P06-8	Felsic rock	30	2.5	4.7
P06-9	Felsic rock (3)	17	5.2	4.9
P06-14	Felsic rock	4.8	5.4	4.5
P06-13	Felsic rock	2.1	1.5	1.5
P06-15	Lakenvalei Quartzite (2)	2.4	18.9	18
P06-16	Lakenvalei Quartzite (2)	7.1	21.5	11
P06-18	Lakenvalei Quartzite (4)	9.0	17.6	18
P06-19	Lakenvalei Quartzite	12	21.2	14
P06-20	Vermont Metapelite (2)	80	2.3	48
P07-49	Felsic rock (2)	67	8.1	5.7
P07-59	Felsic rock	39	2.3	7.0
P07-58	Felsic rock	27	5.1	6.4
P07-52	Felsic rock	8.2	7.7	3.8
P07-53	Felsic rock (2)	4.9	12.1	6.8
P07-50	Lakenvalei Quartzite	0.1	12.8	19
P07-51	Lakenvalei Quartzite (3)	3.5	21.0	12
P07-55	Vermont Metapelite	3.6	7.4	44
P07-56	Vermont Metapelite	34	3.2	105
P07-54	Vermont Metapelite	69	8.2	94
P07-57	Magaliesburg Quartzite	149	22.1	13
West Phepane Small Scale Transect				
P07-34	Mafic rock (2)	33	3.6	10
P07-33a	Mafic rock	26	3.6	12
P07-33b	Mafic rock (2)	26	2.1	12
P07-32	Mafic rock (3)	19	5.3	26
P07-31	Mafic rock	0.8	3.4	19
P07-30	Lakenvalei Quartzite	0.6	8.1	16
P07-29	Lakenvalei Quartzite	19	9.5	13
P07-26	Lakenvalei Quartzite	42	16.1	9.9
P07-28	Lakenvalei Quartzite	51	19.3	17
P07-27	Vermont Metapelite	74	5.4	44

Table 5. Lithium Isotope Compositions and Concentrations (cont.)

Sample	Rock Type	Distance (m)[§]	δ^7Li (‰)	Li (ppm)
West Phepane Large Scale				
P07-12	Mafic rock	241	-0.2	19
P07-11	Mafic rock	124	4.9	59
P07-9	Mafic rock (3)	75	1.7	34
P07-8	Mafic rock	60	3.3	56
P07-7	Mafic rock(2)	35	5.0	51
P07-6	Mafic rock(2)	20	6.0	41
P07-15	Mafic rock	2.6	5.5	19
P07-17	Lakenvalei Quartzite (2)	7.7	15.5	12
P07-14	Lakenvalei Quartzite (2)	10	13.2	22
P07-1	Lakenvalei Quartzite	50	10.6	19
P07-3	Lakenvalei Quartzite (2)	52	9.2	14
P07-5	Vermont Metapelite (2)	54	-6.7	104
P07-16	Vermont Metapelite	71	1.9	85
P07-18	Vermont Metapelite	98	4.0	14
P07-23	Vermont Metapelite	264	4.0	70
P07-24	Vermont Metapelite	303	4.9	67
P07-25	Magaliesburg Quartzite	372	25.5	8.8
Sedimentary Samples				
LV2	Lakenvalei Sandstone		21.7	9.1
LV3	Lakenvalei Sandstone		12.4	8.3
LV4	Lakenvalei Sandstone		9.8	2.3
LV6	Lakenvalei Sandstone		17.3	13
VT1a	Vermont Shale		0.3	142
Mineral Separates				
P06-18	Quartz separate		20.7	25
P06-19	Quartz separate		22.7	21
P07-26	Quartz separate		15.7	16
P07-28	Quartz separate		18.4	18

* Numbers in parentheses indicate the number of measurements (where greater than 1) made on the sample. The numbers reported are averages from the measurements made on each sample.
[§] Measured distances corrected for dip of contact and for variations in elevation.

Table 6. Constraints from Diffusion Models

Traverse	Oxygen best fit $\sqrt{DtK^{-1}}$ (m)	Lithium best fit $\sqrt{DtK^{-1}}$ (m)
East Phepane 06	1.1	2.4
East Phepane 07		6.1
West Phepane small-scale	0.9	9.1
West Phepane large-scale		10.6

East Phepane 06					
Oxygen					
$\sqrt{DtK^{-1}}$				1.1 m*	1.4 m†
	D (m^2/s)	porosity	K_e	t (kyrs)	t (kyrs)
D_{melt}	$9x10^{-13}$	10^{-2}	0.62	2600	4200
D_{fluid}	10^{-8}	10^{-3}	1.86	7.1	12
D_{fluid}	10^{-8}	10^{-5}	1.86	710	1200
West Phepane small					
$\sqrt{DtK^{-1}}$				0.9 m*	1.5 m†
	D (m^2/s)	porosity	K_e	t (kyrs)	t (kyrs)
D_{melt}	$9x10^{-13}$	10^{-2}	0.62	1800	4900
D_{fluid}	10^{-8}	10^{-3}	1.86	3.4	13
D_{fluid}	10^{-8}	10^{-5}	1.86	340	1300

*Best fit diffusive distances.

†Maximum diffusive distances.

Figure Captions

Figure 1. (a) Map of the Bushveld Complex in South Africa modified from Kinnaird et al. (2005), **(b)** Close-up map of Eastern Lobe (dotted line in Figure 1a) showing each igneous zone, the sedimentary rocks of the aureole, and the metasedimentary domes within the Bushveld Complex modified from Clarke et al. (2005).

Figure 2: Google Earth image of the Phepane Dome (dashed area in Figure 1b) showing the location and topography as well as the rock types of the four transects collected.

Figure 3: CL images on left, plane polarized light (PPL) on right. **(a,b)** Image of LV4, Lakenvalei Sandstone. Arrow points to red luminescent authigenic quartz surrounded by non-luminescent cement. Three feldspar grains (F) show brighter (yellow) luminescence. **(c,d)** P07-14: showing bright blue regions (B) surrounded by darker blue luminescence (L) within larger quartz grains. Note fluid inclusions at bottom (arrow) that coincide with the darker blue luminescent overgrowth. **(e,f)** P06-19: non-luminescent (N) fracture cutting brighter luminescing yellow feldspar and blue quartz. Fracturing is visible in PPL, but extent of recrystallization is not. **(g,h)** P06-16: non-luminescent quartz (N) in fluid inclusion-free fractures (arrows).

Figure 4: (a) Photo in crossed polarized light of texture with cuspate plagioclase indicating the presence of partial melt and **(b)** photo of an equilibrium plagioclase (solid-state) with a dihedral angle of 115 degrees. qtz= quartz, pl= plagioclase.

Figure 5: Histograms of dihedral angle measurements. **(top)** 2-D angle measurements for samples from the East (left) and West (right) side of the Phepane Dome. The samples in the top

This is a preprint, the final version is subject to change, of the American Mineralogist (MSA)
Cite as Authors (Year) Title. American Mineralogist, in press.
(DOI will not work until issue is live.) DOI: http://dx.doi.org/10.2138/am-2015-5196

row (P06-15 and P07-30) are within 2 m of the contact, the next two (P06-18 and P07-26) are ~10 m from the contact, and the third row has a sample at 13 m from the contact (P06-19) and 50 m from the contact (P07-1). **(bottom)** 3-D angle measurements using a universal stage.

Figure 6: Oxygen isotopic compositions are plotted with distance from the contact (at x=0) for **(a)** the East Phepane 06 Transect and **(b)** the West Phepane Small Scale Transect. For both graphs open squares represent measured $\delta^{18}O$ values of quartz in quartzite. For the felsic rock, filled triangles represent measured $\delta^{18}O$ values of quartz in felsic rock. For the mafic rock, filled squares represent calculated $\delta^{18}O$ of quartz that would be in equilibrium with the measured $\delta^{18}O$ values of plagioclase at temperatures of 900°C. Measurement uncertainty shown is 2SD. If no error bars are shown on a data point, the uncertainty is less than or equal to the size of the symbol. Smaller inset graphs show the measurements and profiles modeled immediately adjacent to the contact for each traverse. Diffusive distance results ($\sqrt{D_e t K_e^{-1}}$) from the models are shown which best fit to the data and these best fit model profiles for each traverse are shown as black solid lines. The light gray solid lines represent model profiles with the greatest diffusive distance permitted by the data.

Figure 7: Li concentrations of the Bushveld Complex igneous rock (right) and Lakenvalei Quartzite (left) (contact at x=0) in the combined transects on the (a) east side of the Phepane Dome and (b) west side of the Phepane Dome. Points are averages of multiple concentration measurements where available. Error bars are minimum of 10% of measured concentration. Where multiple measurements were made and measured variability was greater, error bars represent the range of the measured concentrations. If no error bars are shown on data point, error is less than or equal to the size of the symbol.

Figure 8: Li isotopic compositions of the Bushveld Complex igneous rock (right) and Lakenvalei Quartzite (left) in the four transects (contact at x=0). Error bars represent 2SD uncertainty. a) East Phepane traverse 06, b) East Phepane traverse 07, c) West Phepane large-scale traverse, d) West Phepane small-scale traverse. The black lines represent model profiles that best fit the data.

Figure 1a
Ireland and Penniston-Dorland

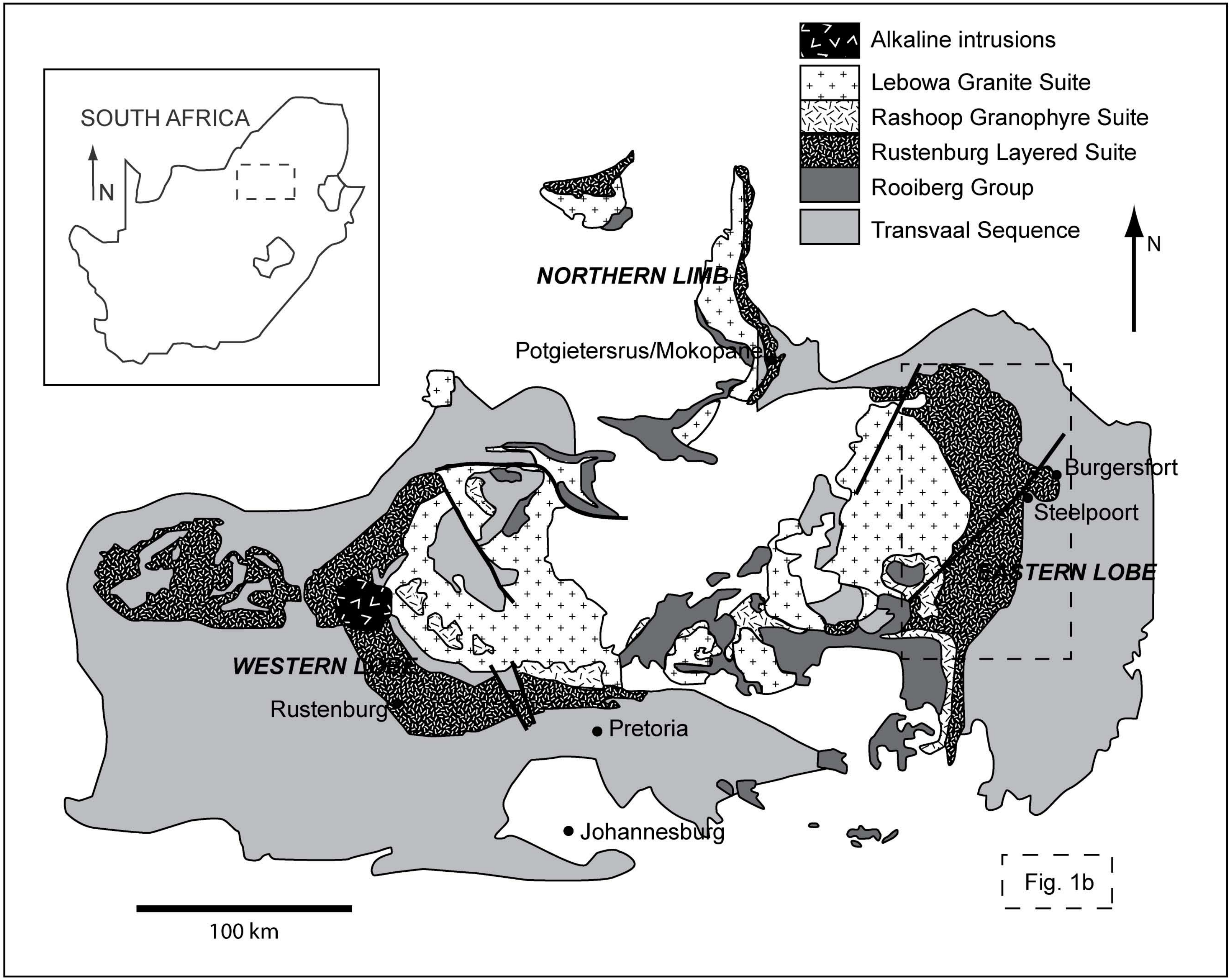

Figure 1b
Ireland and Penniston-Dorland

Bushveld Complex
- Upper Zone
- Main Zone
- Critical Zone
- Lower Zone
- Marginal Zone
- Aapiesdoring Peridotite

Transvaal Supergroup
- Pretoria Group (undifferentiated)
  - Houtenbek Formation
  - Steenkampsberg Formation
  - Nederhorst Formation
  - Vaalian Diorite
  - Lakenvalei Formation
  - Vermont Formation
  - Magaliesberg Formation
  - Silverton Formation
  - Dashoop Formation
  - Boshoek Formation
  - Timeball Hill Formation
- Chuniespoort Group

Alkaline Igneous Rock
- Nebo Granite
- Dullstroom Formation
- Rooiberg Group and Rashoop Granophyre Suite
- Spitskop Alkaline Complex

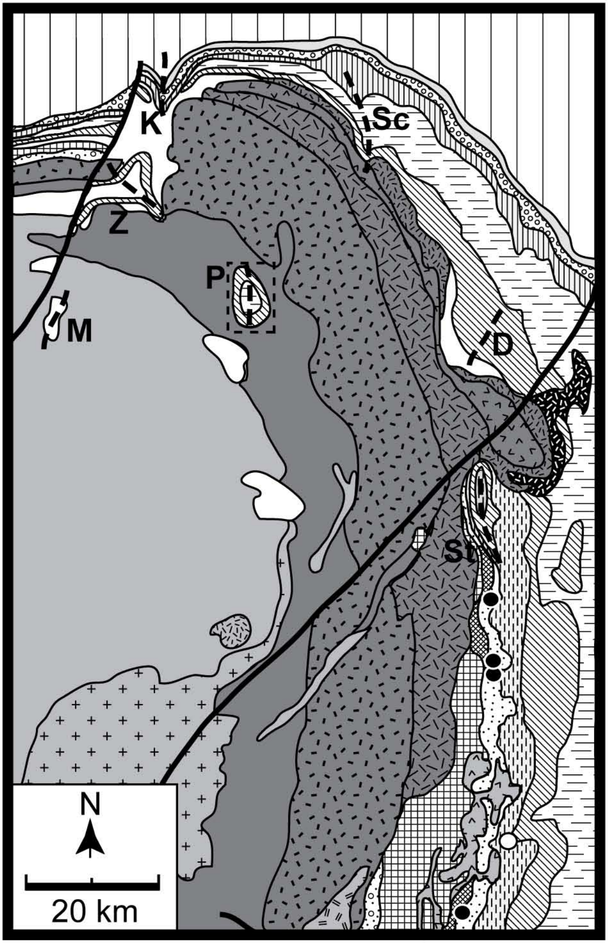

Domes of the Eastern Lobe:
M= Malope; Z= Zaaikloof; K= Katkloof; Sc= Schwerin;
P= Phepane; St= Steelpoort; D= Derde Gelid

Major faults
Axial trace of Dome
(Fig. 2)

Vermont Sample
Lakenvalei Samples

Figure 2
Ireland and Penniston-Dorland

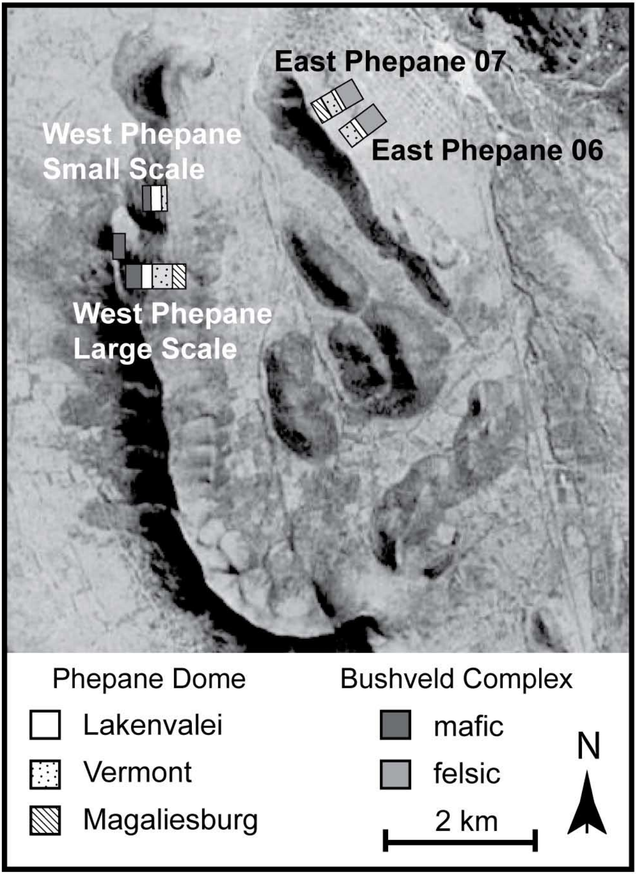

Figure 3
Ireland and Penniston-Dorland

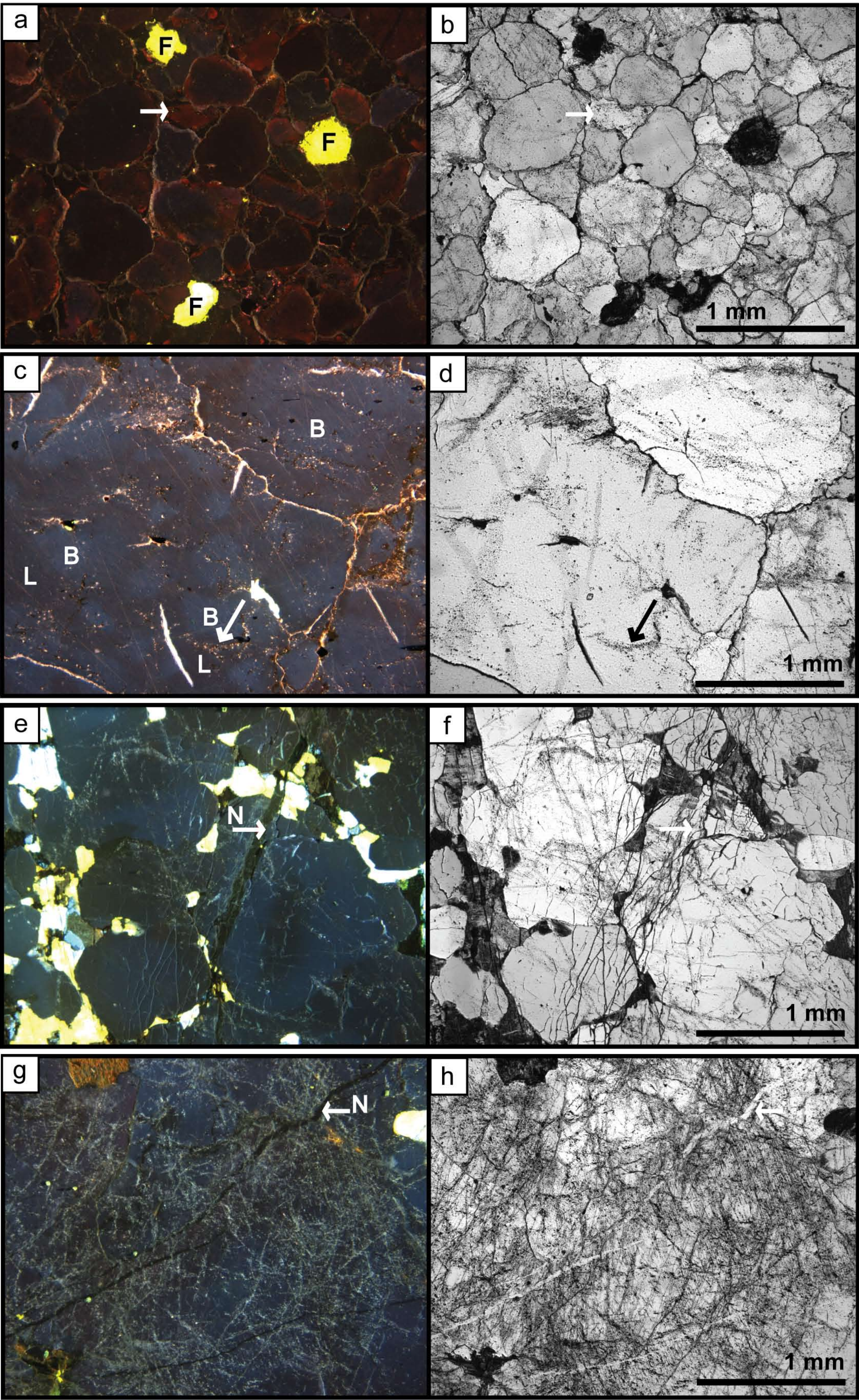

Figure 4
Ireland and Penniston-Dorland

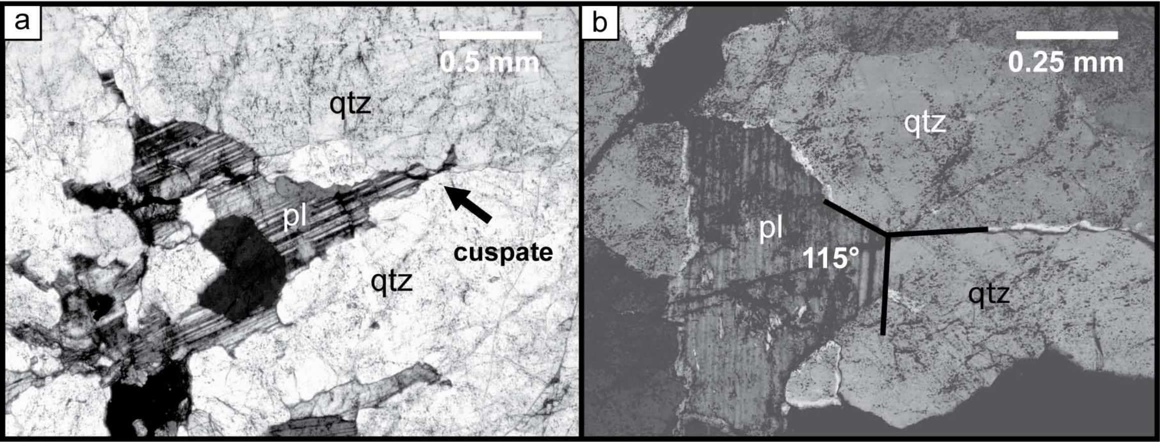

Figure 5
Ireland and Penniston-Dorland

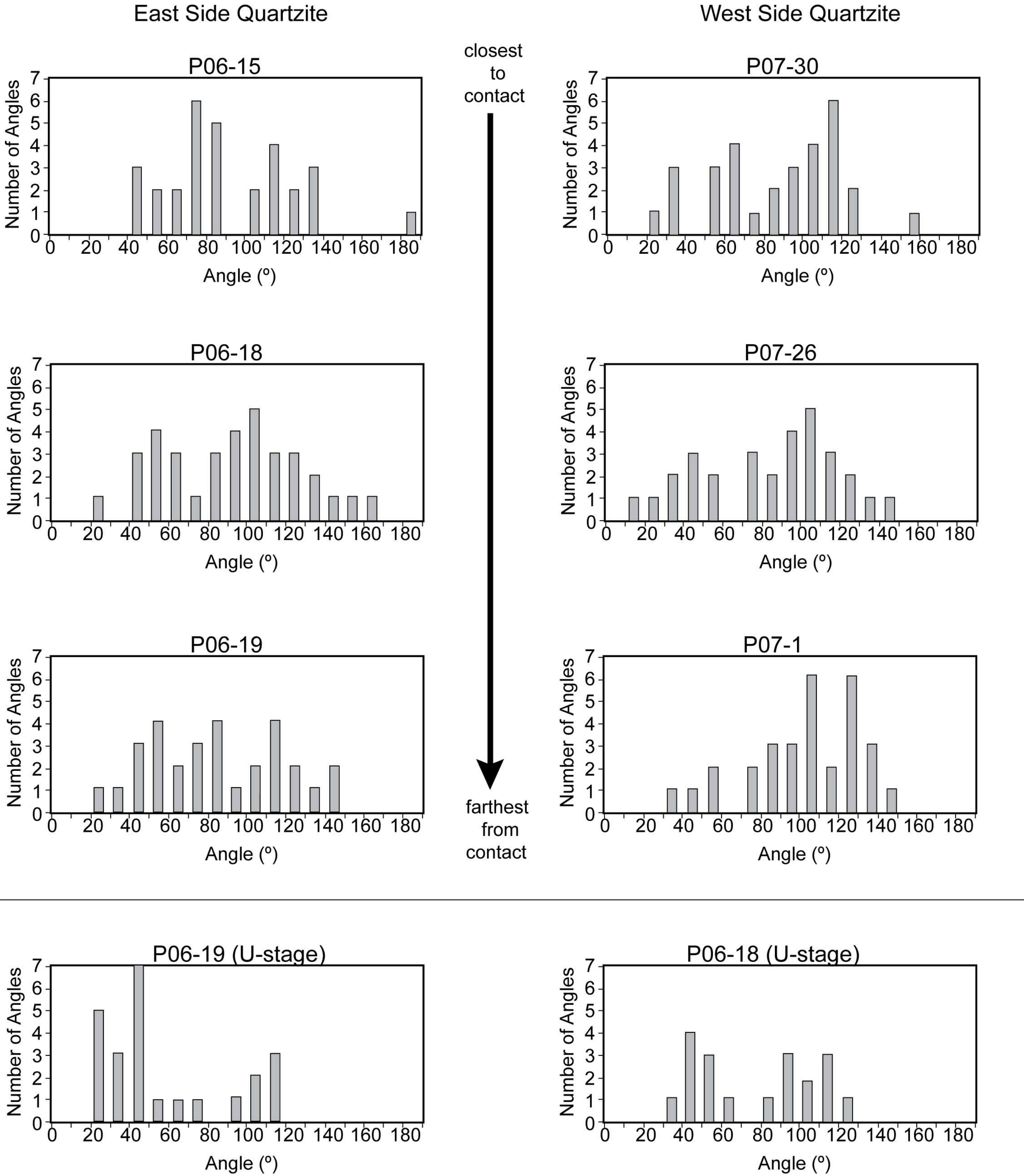

Figure 6
Ireland and Penniston-Dorland

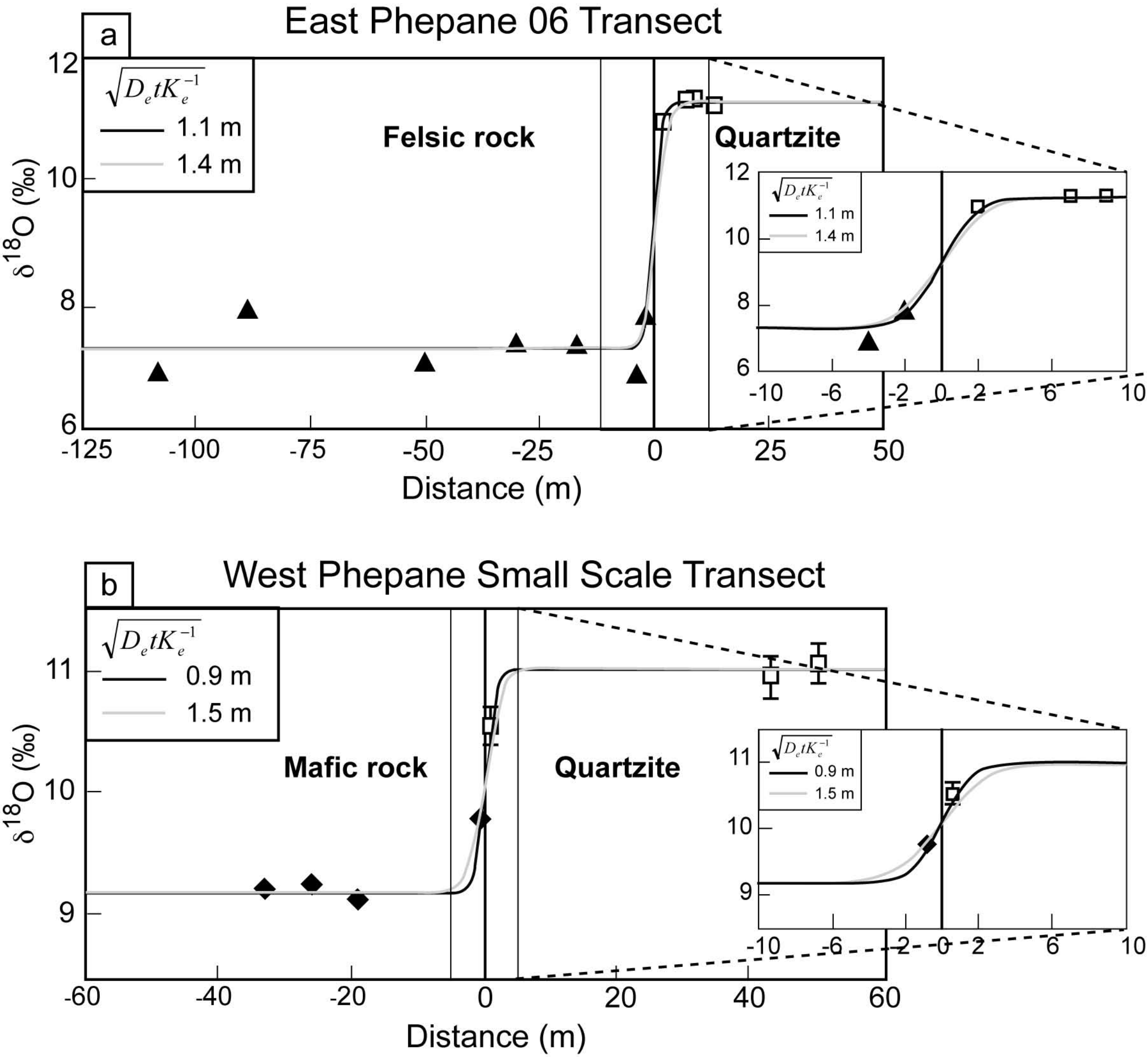

Figure 7a
Ireland and Penniston-Dorland

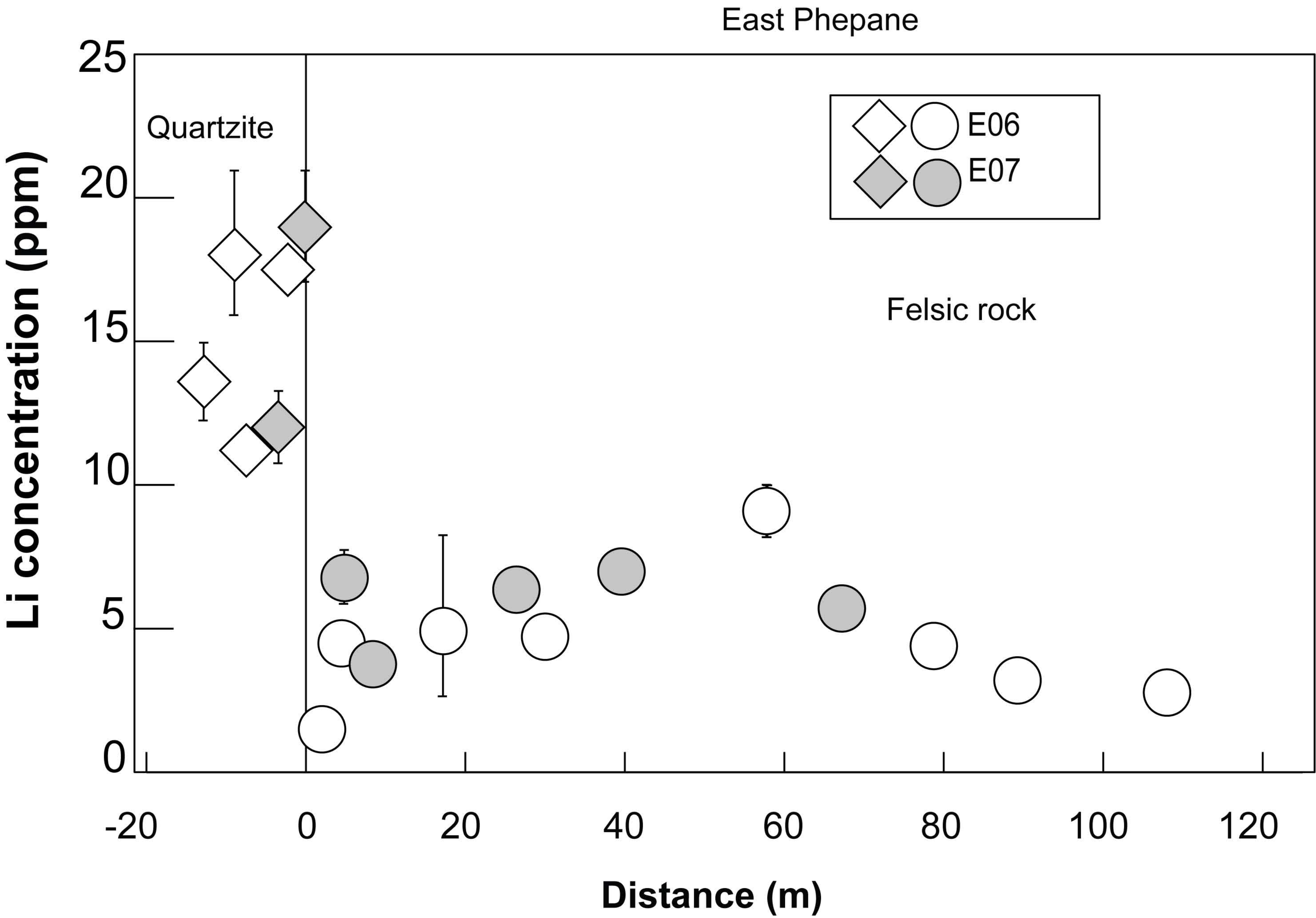

Figure 7b
Ireland and Penniston-Dorland

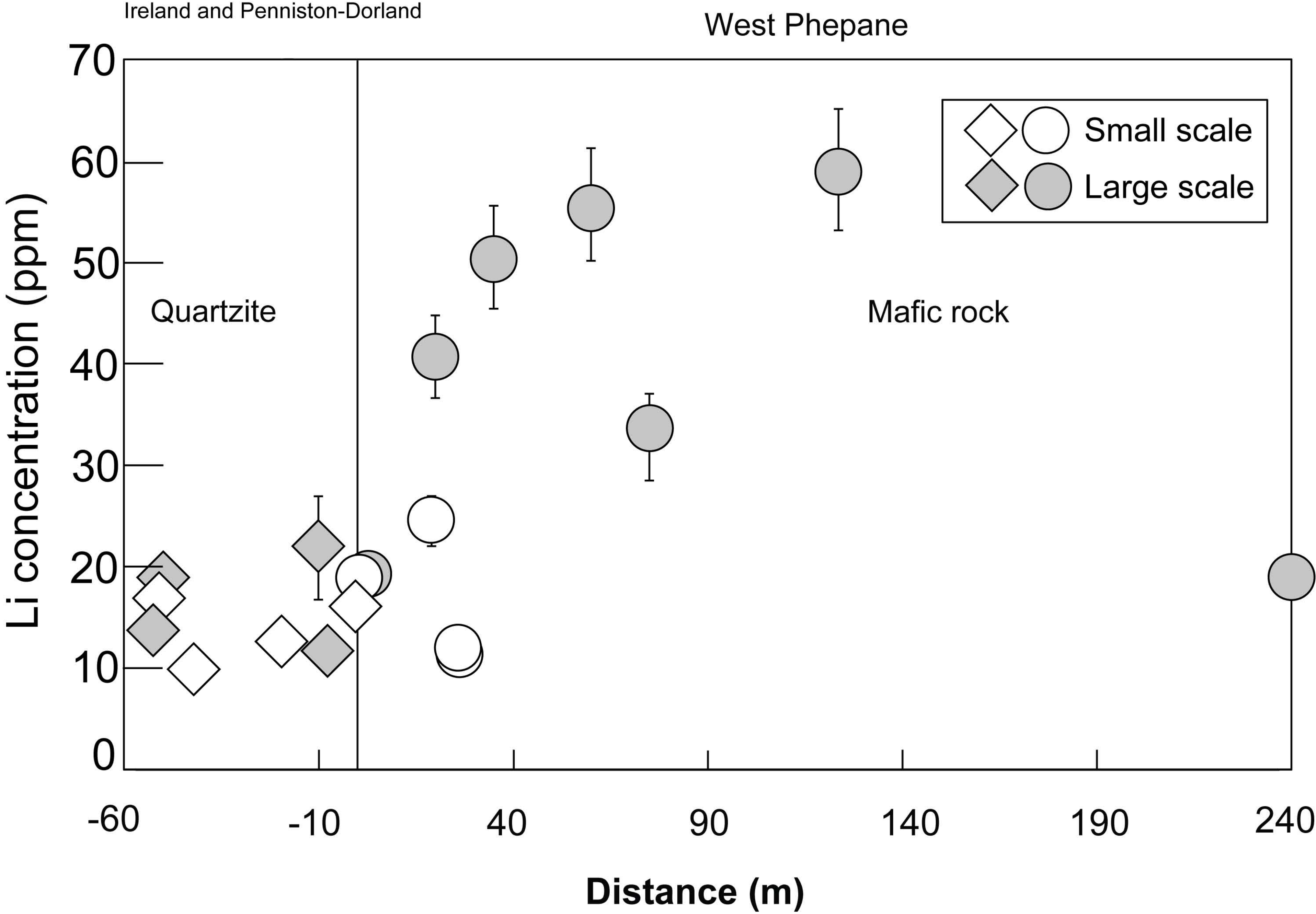

Figure 8
Ireland and Penniston-Dorland